Erythropoietin enhances postnatal hippocampal mitochondrial content, function, and cognition

Robert Jacobs
University of Colorado Colorado Springs https://orcid.org/0000-0003-0180-8266
Mostafa Aboouf
Institute of Veterinary Physiology, Vetsuisse-Faculty University of Zurich
Christian Arias Reyes
Université Laval https://orcid.org/0000-0003-2802-8112
Sofien Laouafa
University Laval
Christina Koester-Hegmann
University of Zurich
Markus Thiersch
University of Zurich https://orcid.org/0000-0002-9118-8285
Jorge Soliz
Institute Universitaire de Cardiologie et de Pneumologie de Québec (IUCPQ)
Max Gassmann
University of Zürich
Edith Schneider Gasser (edith.schneidergasser@uzh.ch)
University of Zurich https://orcid.org/0000-0001-7371-1477

Article

Keywords: oxidative phosphorylation, erythropoietin receptor, spatial memory, short-term memory, Erk1/2, AKT.

Posted Date: September 1st, 2020

DOI: https://doi.org/10.21203/rs.3.rs-62548/v1

Version of Record: A version of this preprint was published at Communications Biology on August 5th, 2021. See the published version at https://doi.org/10.1038/s42003-021-02465-8.

Erythropoietin enhances postnatal hippocampal mitochondrial content, function, and cognition

Robert A. Jacobs[1,5], Mostafa A. Aboouf[1,6], Christian Arias-Reyes[4], Sofien Laouafa[4], Christina Koester-Hegmann[1,2], Markus Thiersch[1,6], Jorge Soliz[4], Max Gassmann[1,6], and Edith M. Schneider Gasser[1,2,3,*]

1- Institute of Veterinary Physiology, Vetsuisse-Faculty University of Zurich Winterthurerstrasse 260
2- Institute of Pharmacology and Toxicology, University of Zurich, Zurich, Switzerland.
3- Center for Neuroscience Zurich (ZNZ), Zurich, Switzerland
4- Institut universitaire de cardiologie et de pneumologie de Québec, Centre Hospitalier Universitaire de Québec (CHUQ), Faculty of Medicine, Université Laval, Québec, QC, Canada.
5- University of Colorado Colorado Springs, Department of Human Physiology & Nutrition, Colorado Springs, Colorado, USA
6- Zurich Center for Integrative Human Physiology (ZIPH), University of Zurich, Zurich, Switzerland

Keywords: oxidative phosphorylation, erythropoietin receptor, spatial memory, short-term memory, Erk1/2, AKT.

Running title: Erythropoietin on hippocampal mitochondrial respiration and cognition.

***Corresponding author:** edith.schneidergasser@uzh.ch; Institute of Veterinary Physiology, University of Zurich, Switzerland; +41446358814

ABSTRACT

It is increasingly evident that mitochondria are crucial in regulating neurodevelopment, brain function and cognition. Erythropoietin (EPO) has been shown to improve mitochondrial function and cognition following brain damage and in patients with neurological disorders. However, potential EPO-mediated influence(s) on hippocampal mitochondrial function during postnatal development and it corresponds to enhanced cognition is unknown. Here we show in mice, that EPO receptors (EpoR)s express postnatally in the CA1 pyramidal cells of the hippocampus reaching a zenith at puberty (postnatal (P) age 21). Constitutive neuronal EPO overexpression increases hippocampal Erk1/2 and AKT phosphorylation along with increases in cellular respiration and mitochondrial content by the third postnatal week of development. Indices of cellular oxidant balance do not appear altered by higher respiratory potentials and greater mitochondrial content. Finally, EPO overexpression also enhances hippocampal-dependent learning and memory at early adulthood (P60). Collectively, this data identifies a novel function for EPO signaling, promoting improvements in hippocampal-specific mitochondrial function and cognition during postnatal development and early adulthood.

INTRODUCTION

Erythropoietin (EPO) continues to emerge as one of the most promising neuroprotective agents with vast clinical relevance. EPO and its receptor (EpoR) are expressed in the brain [1], where it exhibit neuroprotection following traumatic injury, hypoxia-ischemic insults, excitotoxicity, and inflammatory brain injury [2,3]. More specifically, EPO has been shown to prevent hippocampal neurodegeneration and attendant cognitive impairment in diabetic mice [4], as well as reduce long-term spatial memory deficits across various animal models of neonatal brain injury [5,6]. In humans, EPO has been shown to enhance memory retrieval in healthy individuals in addition to those suffering from various neurodegenerative diseases and dementia by increasing hippocampal plasticity [2,7-10], along with improved neurogenesis [7,11-13]. The neuroprotective potential of EPO may also extent to neonatology, since EPO has been reported to reduce perinatal brain injury [14,15] and improve neurological outcomes in very prematurely born neonates [14,16,17].

EPO-mediated neuroprotective mechanisms involve the activation of multiple downstream transcriptional regulators, including Erk1/2 and PI3K/AKT [6], that concomitantly upregulate anti-apoptotic, anti-inflammatory, anti-oxidative and anti-cytotoxic pathways [6,14,15]. The cellular responsibilities of these pathways (i.e. apoptosis, redox balance, cytotoxicity, and inflammation) relate to one another in their dependence on mitochondrial control. The importance of mitochondria in neuronal development and function is highlighted by their pivotal role in promoting neuronal differentiation, neurotransmission and synaptic pruning [18]. The close relationship mitochondria share with neurodevelopment and cognition is also evidenced by the influence of mitochondrial

morphology and function on synaptic vesicle pool regulation, spatial memory, and working memory throughout neuronal maturation [19,20]. The mechanism(s) of EPO-mediated neuroprotection appear to function at least somewhat through mitochondrial. EPO has been reported to support neuronal mitochondrial activity and to prevent memory impairment in animal models of multiple sclerosis, sleep deprivation, neurodegeneration and brain injury [21-25]. Furthermore, EPO prevents neurobehavioral deficits in the hippocampus of young rats exposed to intermittent hypoxia [26], as well as a murine model of sleep apnea [27] by managing oxidant strain on the cell. However, many questions relating to the potential of EPO in regulating brain mitochondrial respiratory control and development remain to be answered. The hippocampus undergoes substantial neuronal differentiation, synaptogenesis, and neuronal circuit formation throughout postnatal development. The mitochondrial influence in promoting these processes is unexplored. Additionally, whether EPO, in parallel to the activation of neuroprotective pathways, modulates mitochondrial functions during postnatal maturation and improves hippocampal-mediated cognitive functions is yet unknown.

Using a transgenic mouse line (Tg21) constitutively overexpressing EPO specifically in neurons, we set out to identify the impact of EPO on mitochondrial respiration and oxidant balance in the hippocampus throughout postnatal development until adulthood. To differentiate between possible qualitative vs quantitative influences on mitochondrial function, we examined various measures of mitochondrial protein expression and activity as surrogates for mitochondrial content. We lastly examined how CNS overexpression of EPO, along with potential mitochondrial alterations, associate with targeted area-specific cognitive performance in early adulthood. Collectively, our results show that CNS-specific

EPO overexpression primarily influences postnatal hippocampus as increases in EPO receptor (EpoR) expression is mainly limited to CA1 pyramidal cells during this developmental window. EPO-mediated upregulation of Erk1/2 and AKT phosphorylation in pyramidal CA1 throughout postnatal development appear to correspond with attendant improvements in mitochondrial function and hippocampal-specific cognition.

RESULTS

rhEPO overexpression in the brain is highest during postnatal development while EpoR expression in WT and Tg21 mice increase similarly throughout postnatal development and only in the hippocampus

No differences were observed between genotypes (WT vs Tg21) regarding spleen weight, hematocrit, hemoglobin, or plasma EPO concentrations at P60 (Fig. 1a). mEPO expression was poorly detected in the brain of WT or Tg21 mice while rhEPO was only detected in the brain of Tg21 mice at P60 (Fig. 1b). Constitutive overexpression of rhEPO was restricted to the brain of Tg21 groups (P5 and P21). There was a transient elevation detected in the liver at P5 but no differences in kidney or spleen (Fig. 1c).

Hippocampal total EPO expression was significantly higher in Tg21 vs WT mice across all ages (Fig. 1d). Specifically, average EPO protein expression in WT mice was 47±3 pg/mg immediately after birth (P1), which then decayed rapidly with postnatal development to adulthood. Alternatively, hippocampal EPO concentrations in Tg21 mice were 2-fold higher at P1, 4-fold higher at P3, and 20-fold higher at P7 and P14 as compared to WT mice. Thereafter, EPO overexpression in Tg21 animals diminished to a 14-fold versus WT controls at P21, and then to a sustained 4-fold in adulthood (P90). Hippocampal EpoR mRNA expression increased across postnatal development in both

WT and Tg21 mice, reaching a 3-fold increased expression at P21 with no observable differences between genotypes (Fig. 1e). Negligible measures of cortical EpoR mRNA expression were detected after birth or throughout development with no differences between genotypes, except for a transient increase in WT mice at P14 (Fig. 1f). FISH analysis showed abundant expression of mEpoR mRNA in the corpus amonis (CA)1 pyramidal cell layer of the hippocampus and negligible expression in the cortex in both genotypes at P60 (Fig. 1g). This data verifies our transgenic model, which overexpresses EPO specifically in the brain with no effect on EpoR expression when compared to WT controls. Also, it shows that EpoR transcripts increase in the hippocampus and remain largely unchanged in the cortex, throughout postnatal development. By P21, EpoR mRNA reaches its greatest expression, staying high until adulthood (P60) in hippocampal CA1 pyramidal neurons while unidentifiable in the cortex.

EPO overexpression in the CNS activates Erk1/2 and AKT in the hippocampus

EPO/EpoR cellular signalling, acts through multiple pathways including Erk1/2 and AKT. Therefore, we analysed total extracellular signal-regulated kinase (Erk)1/2 and AKT protein expression along with phosphorylated (p) Erk1/2 and AKT expression throughout postnatal development (Fig. 2). Total Erk1/2 (Fig. 2 a-b) and p-Erk1/2 (Fig. 2 c-d) band intensities were normalized to vinculin expression. There were no differences in total Erk1/2 expression between WT and Tg21 mice (Fig. 2b). Alternatively, p-Erk1/2 was at least 2-fold higher in Tg21 mice across all postnatal ages (Fig. 2d). The greatest difference in p-Erk1/2 between genotypes, identified primarily by the 42 kDa band, occurred at postnatal ages P3 and P21 (Fig. 2c). Fluorescent western blot analyses of total AKT (red) and p-AKT (green) expression (Fig. 2e) showed a 2-3 fold increase in p-

AKT over total AKT in Tg21 mice (Fig. 2e lower bands and Fig. 2g) without change in total AKT (Fig. 2e upper band showing only the red channel and Fig. 2f). AKT was normalized to β actin. No change in Erk1/2 and AKT was observed throughout development in either genotype. p-AKT was also unaltered across development in Tg21 mice but an increase in WT from P3 to P7 was observed. Along with the data presented in figure 1, this data suggests that EPO activation of Erk1/2 and AKT occurs in the hippocampus without influencing total protein expression of theses transcriptional regulators.

CNS EPO overexpression influences mass-specific respiratory control in postnatal hippocampus

Measurements of mass-specific (pmol O_2/s * mg ww) leak respiration with the addition of malate + octanoylcarnitine, or ADP across postnatal development in hippocampus did not differ between genotypes and OCR did not increase with the addition of malate + octanoylcarnitine, or ADP (Fig. 3b, L_N). However, following the titration pyruvate and glutamate P_{CI} OCR was higher in Tg21 hippocampus at ages P14 and P21 (Fig. 3b, and 3c). No changes in P_{CI} OCR in cortex and brainstem from Tg21 mice were observed (Fig. S1). In the hippocampus, respiration also increased in both genotypes following the addition of succinate with P_{CI+CII} OCR significantly higher in the Tg21 mice at P21 (Fig. 3c and 3d). With the addition of FCCP again E_{CI+CII} OCR observed was higher at P14 and P21 in the Tg21 mice (Fig. 3e). Respiratory inhibitors rotenone and antimycin A each respectively reduced respiratory rates in both genotypes with no identifiable difference in E_{CII} (2-way ANOVA, $F(1,66) = 0.32$, $p = 0.54$) or ROX (2-way ANOVA, $F(1,66) = 0.545$, $p = 0.436$) between genotypes.

There was a main age independent effect of genotype on mass-specific OCRs, with an increase observed as age advanced (Fig. 3b, 2-way ANOVA, $F(3,264) = 372.6$, $p < 0.0001$). In general, the age-associated increase in OCR occurred earlier in the postnatal development of Tg21 mice when compared to their WT counterparts. Specific intra-genotypic differences in respiratory states across ages included: P_{CI} (Fig. 3c; WT: P3, P7 and P14 less than P21 and P60; 1-RM ANOVA, $F(4,32) = 25.2$, $p < 0.0001$; and Tg21: P3 and P7 less than P14, P21 and P60; 1-RM ANOVA, $F(4,34) = 24.52$, $p < 0.0001$); P_{CI+CII} (Fig. 3d; WT: P3 less than P14, P21 and P60; P7 less than P21 and P60; and P14 less than P21 and P60,; 1-RM ANOVA, $F(4,32) = 16.84$, $p < 0.0001$); and Tg21: P3, P7 less than P14, P21 and P60; 1-RM ANOVA, $F(4,36) = 22.47$, $p < 0.0001$); and E_{CI+CII} (Fig. 3e; WT: P3, P7 less than P21 and P60, and P3 less than P14; 1-RM ANOVA, $F(4,32) = 10.96$, $p < 0.0001$; and Tg21: P3 and P7 less than P14, P21, and P60; 1-RM ANOVA, $F(4,36) = 30.78$, $p < 0.0001$). E_{CII} increased with age equally in WT and Tg21 (P3 and P7 less than P14, P21 and P60; 1-RM ANOVA, $F(4,66) = 8.078$, $p < 0.0001$). Observed age-specific measures from both genotypes are similar to [28-30] or higher than [31] analogous respiratory state OCRs previously reported when respiring brain samples from C57BL/6 mice and/or Winstar rats. Collectively, this data suggests that the overexpression of EPO in the hippocampus facilitates greater respiratory capacity earlier in postnatal development compared to WT controls, having a peak at P21.

Mitochondrial content in hippocampus through postnatal development is increased in Tg21 mice

A surrogate of mitochondrial content as indicated by COX activity differed between genotypes throughout postnatal development, with higher measures observed at P14,

P21, and P60 in Tg21 animals (Fig. 4a). Mitochondria-specific respiratory analysis (mass-specific respiration normalized to COX activity) helps distinguish qualitative alterations in mitochondrial function that may influence respiratory control from quantitative differences in mitochondrial content that instead characterize variations in respiratory control. In general, age-matched mitochondria-specific OCRs were similar between genotypes across respiratory states (Fig. 4b). There was a main effect of age on mitochondria-specific OCRs for P_{CI} (WT: 1-RM ANOVA, $F(4,31) = 6.768$, $p = 0.0005$; and Tg21: 1-RM ANOVA, $F(4,34) = 5.009$, $p = 0.0028$); P_{CI+CII}(WT: 1-RM ANOVA, $F(4,39) = 3.183$, $p = 0.0235$; and Tg21: 1-RM ANOVA, $F(4,42) = 3.486$, $p = 0.0151$=); and E_{CI+CII} (WT: 1-RM ANOVA, $F(4,39) = 3.827$, $p = 0.012$; and Tg21, 1-RM ANOVA, $F(4,42) = 4.893$, $p = 0.0025$). However, there did appear to be some nuance as to how respiratory control and mitochondrial content adapted throughout postnatal development between genotypes. COX activity did not increase in WT mice until P21 while Tg21 mice demonstrated a gradual increase from P3 to P21 (Fig. 4a). Similarly, P_{CI} and P_{CI+CII} OCRs increased unevenly in WT animals with the greatest increase observed between P14 and P21 whereas Tg21 animals displayed a gradual increase to P21 where they displayed their highest rates of respiration (Fig. 4c and d). When normalizing respiratory state OCRs to COX, differences between genotypes were lost (Fig. 4b). This data suggests that mass-specific OCR differences are most likely attributable to quantitative disparities in mitochondrial content between genotypes opposed to qualitative variations in mitochondrial function.

To support these findings, we also examined the expression of various mitochondrial proteins (Fig. 5). An increase in voltage-dependent anion channel 1 (VDAC1)-

immunoreactivity (Fig. 5a and b) was observed it Tg21 mice, reaching a 4.9-fold increase at P14 and 1.6-fold increase at P21 (Fig. 5b). VDAC1 is the most abundant protein of the outer membrane of mitochondria. Expression of various mitochondrial proteins specific to the electron transport system, were higher in Tg21 mice compared to WT throughout postnatal development (Fig. 5c to h). Specifically, complex I (NDUFB8) immunoreactivity was 2.7-fold higher at P7 and 4-fold higher at P14 (Fig. 5d), complex III (UQCRC2) immunoreactivity was 13.7-fold higher at P7 (Fig. 5f), complex IV (COX-IV) immunoreactivity was 3.9-fold higher at P7, and 2.9-fold higher at P14 and P21, and 2-fold higher at P60 (Fig. 5g), and complex V (ATP5A) immunoreactivity was 3.2-fold higher at P7 in Tg21 mice (Fig. 5h). Opposingly, there was no significant difference in complex II (SDHB) immunoreactivity at any age between genotypes (Fig. 5e). Collectively, this data supports our previous data suggesting mitochondrial content is higher in Tg21 animals throughout portions of postnatal development when compared to WT. Interestingly the high increase in complex III, complex IV and complex V protein expression at P7 in Tg21 mice did not result in any increase in mitochondrial respiration, therefore, the increase in mass respiration at P14 and P21 mainly results from increase in mitochondrial content.

EPO brain overexpression promotes an increase of super oxide dismutase 1 (SOD1) activity at P14 with no differences in ratio of cytosolic NOX to SOD1

As electron passage through the transport chain results in reactive oxygen species (ROS) production and oxidant signalling through transcriptional regulators such as ERK in the hippocampal CA1 area [32,33], we were also interested in examining EPO's parallel influence on cytosolic superoxide production and scavenging via NOX and SOD1 activity,

respectively. As most significant differences in mass-specific respiration occurred at P14 and P21 between genotypes, NOX and SOD1 activities were assessed at these time points (Fig. 6). No significant EPO-mediated influence on NOX activity was identified (Fig. 6a), but Tg21 mice showed greater SOD1 activity at P14 when compared to age-matched WT counterparts (Fig. 6b). No differences in the ratio NOX/SOD1 between genotypes were observed (Fig. 6c). This data extends upon the respiratory findings suggesting that the any increase in respiration throughout postnatal development does not appear to share a parallel drive to increase oxidant load, as there was no observable differences in ratio of cytosolic NOX to SOD1 activities between genotypes, although SOD1 activity was higher in Tg21 animals at P14.

CNS EPO overexpression enhances hippocampal-dependent spatial navigation and memory

Young adult mice from both genotypes successfully learned to find the hidden platform during acquisition phase prior to running the Morris water maze (MWM) test, as demonstrated by the escape latency (Fig. 7a) and swimming path length (Fig. 7b). A faster escape latency was observed in Tg21 mice beginning on day 2 (d2). The swimming path length was not different between genotypes during the acquisition phase (Fig. 7b). However, indication of enhanced learning in Tg21 was evident when comparing to WT controls across days, with Tg21 mice showing a longer swim path on d1, negligible differences in swim path on d2, and shorter swim paths on d3 and d4 (Fig. 7b). Additionally, Tg21 mice exhibited faster swim speeds than WT controls across all days (Fig. 7c). During the reversal trial (d5), both groups showed increased preference for the training quadrant, and this preference was stronger in Tg21 animals (2-way ANOVA,

F(1,88)=105, $p< 0.0001$). Additionally, Tg21 mice presented shorter escape latency (Fig. 7d); shorter swim path length (Fig. 7e), and faster swim speed (Fig. 7f) when finding the new hidden platform location. These results demonstrate that Tg21 mice have improved spatial learning and memory when compared to WT controls.

The cognitive impact of EPO on recognition memory was assessed with the novel object recognition (NOR) tasks (Fig. 8a). Mice were habituated to learn the location and become familiar with two equal objects over a single 5 min learning event. Subsequently, short-term, and long-term memory was examined when testing the recognition of a novel object after 1h and 24 h ITIs, respectively (Fig. 8a). During the habituation phase, Tg21 animals explored the empty arena more intensively than WT mice, resulting in more total locomotor activity (4.96 ± 6.8 m/min vs. 3.97 ± 6 m/min, respectively, t-test, $p < 0.001$). During the training phase, total object exploration time was similar between genotypes. In the short-term memory test, both WT and Tg21 mice spent more time exploring the novel object. However, Tg21 mice exhibited a stronger preference for the novel object reflected by an object discrimination index above 0.5 (Fig. 8a). Long-term memory was then tested 24 h later when the mice were given 5 min in the arena with a novel displaced object. In this task, both genotypes equally recognized the novel object with a similar ODI of 0.28 ± 0.18 for WT and 0.25 + 0.2 for Tg21. Although this test is not exclusively hippocampal, as visual cues are involved in task analysis, it is a valid test to assess cognition in young adult mice with the speed in learning locations highlighting cognitive flexibility. Finally, T-maze working memory, which involves areas of the brain other than the hippocampus, showed no differences in spontaneous alternation between genotypes

(Fig. 8b), but Tg21 mice were faster in the choice (10.13 ± 0.74 s for WT and 7.37 ± 0.70 s for Tg21).

Collective cognitive testing demonstrates that EPO overexpression improves speed performance, hippocampal mediated spatial learning and memory, and short-term memory in mice, but long-term memory and working memory remained unaltered.

DISCUSSION

The present study aimed to examine the effects of constitutive CNS EPO overexpression on mitochondrial characteristics throughout postnatal development and cognition in young adult mice. Our reported findings show that CNS EPO overexpression primarily influences hippocampal postnatal development. Negligible measures of EpoR expression soon after birth do not increase throughout postnatal development in the cortex as they do in the hippocampus, with the greatest expression identified at puberty (P21) in CA1 pyramidal neurons across control and transgenic genotypes alike. Furthermore, constitutive CNS EPO overexpression was shown to upregulate p-Erk1/2 and p-AKT in the hippocampus without any influence on total protein expression. EPO-mediated influence on the CNS throughout postnatal development also corresponded to earlier (~P14) increases in hippocampal mitochondrial respiration most likely through mitochondrial content expansion with no evidence of dysfunction in mitochondrial or cytosolic oxidant production. Lastly, CNS EPO overexpression improved hippocampally dependent spatial navigation and short-term memory by early adulthood (P60). We conclude that EPO functions in the hippocampus through CA1 cells by enhancing

mitochondrial energetics in postnatal neurodevelopment and early adulthood thereby facilitating improved cognition.

The coordination of EPO and EpoR expression in the brain and influence on cellular signaling pathways

Our transgenic mouse model (Tg21), which overexpresses rhEPO exclusively in neuronal tissue [34,35], showed the greatest increase in hippocampal EPO expression between genotypes (20-fold) at P14. Alternatively, there were no major variations in EpoR mRNA expression between WT controls and Tg21 animals throughout development. Thus, EPO-mediated cellular signaling through the EpoR in the brain is dependent of ligand concentration. EpoRs, primarily expressed by CA1 pyramidal neurons, gradually increase throughout postnatal development reaching a 3-fold increase compared to P1 by postnatal age P14 and maximal expression at puberty (P21). Transcriptional regulation of EpoR expression in these cell types is not yet defined. The steady and equivalent transcriptional increase in hippocampal EpoR mRNA between genotypes suggests an essential role of intracellular receptor pools to manage basal and acute EPO-dependent cellular signaling in the brain, similar to the hematopoietic system [36]. The CA1 and CA3 regions of the hippocampus undergo rapid maturation during the second postnatal week that parallel dendritic arborisation, axon growth, spine density, and synaptogenesis in CA1 pyramidal cells [37]. GABAergic synapses also form within the postsynaptic populations of CA1 neurons at this age [38]. A transient hippocampal hyperexcitability in the second postnatal week has been reported as a result of axonal remodeling [39]. Hyperexcitability causes brief episodes of hypoxia in CA1 pyramidal neurons [40]. Therefore, it is probable that these transient episodes of local hypoxia signal the

upregulated expression of EpoRs in CA1 pyramidal cells at this age. This evidence of EpoR expression primarily concentrating in postmitotic pyramidal cells in the CA1 area as postnatal development progresses introduces previously unexplored potential for and dependence on EPO signaling in these cells.

In this study EPO overexpression in the developing postnatal hippocampus showed no influence on total Erk1/2 or AKT protein expressions but was associated with higher measures of p-Erk1/2 and p-AKT, consistent with the known downstream signaling from EPO-EpoR activation [41]. Both Erk1/2 and AKT pathways have been reported to be involved in neuronal survival [42-44], neuronal differentiation [45], synaptic plasticity and cognitive function relating to the hippocampus [46-48]. Mitochondrial-specific Erk1/2 translocation in the developing rat brain is thought to help orchestrate nuclear proliferation and differentiation in response to energetic and redox status [49]. Previous research has shown that N-metyl-D-aspatate (NMDA) activation, which is required for synaptic plasticity in the hippocampus, results in greater ROS production and concomitant signaling through ERK in the CA1 area [33] and mitochondrial ROS has been shown to regulate the inhibitory strength GABAergic synapses in hippocampus [50]. Moreover, NOX in synaptic neurons of the hippocampus are required for the activation of Erk1/2 and, thus, are suggested to be involved in hippocampal long-term potentiation [33]. In this study, the evidence of increased p-Erk1/2 along with no change in mitochondrial ratio of cytosolic NOX to SOD1 activity leads us to deduce that cellular oxidant signalling may have improved without any associated burden of oxidant strain. Increased oxidant strain would have ultimately been detrimental to neural maturation and hippocampal function [51-53], neither of which were observed in the current study.

EPO overexpression increases respiration and mitochondrial content in developing postnatal hippocampus

Mitochondria are essential for neuronal development, excitability, and survival in addition to synaptic signaling and plasticity [54,55]. Mitochondria also influence cognition. Cannabinoid-induced amnesia develops in part from reduced hippocampal respiration through mitochondrial specific type-1 cannabinoid receptor regulation while manipulations shown to maintain hippocampal bioenergetics also minimize associated memory impairments [56]. EPO has also been shown to induce plasticity at hippocampal synapses and improves memory retrieval [7,9,57]. We do not believe these empirically established roles of EPO on mitochondrial physiology and cognition to be a coincidence. EPO has already been shown to increased mitochondrial biogenic signaling and/or improve oxidative metabolism in adipose tissue [58], myocardial tissue along with Erk1/2 and AKT1 activation [59], and skeletal muscle [60] from mice as well as human skeletal muscle [61,62]. Thus, we postulated that the cognitive benefits of EPO may be facilitated through functional differences in hippocampal mitochondria throughout neuronal maturation, which would in turn enhance synaptic plasticity and consequently improve spatial memory. Like hippocampal EpoR expression, we generally observed progressive respiratory increases in the hippocampus throughout postnatal development with peak values observed at P21 in both WT control and Tg21 mice. However, EPO appeared to hasten mitochondrial maturation as respiratory rates reached statistically similar values to those measured in young adults (P60) by P14 in Tg21 but not WT mice. Changes in mitochondrial content were like respiration as evidenced by the increased COX activity and mitochondrial protein expression that achieved peak values at P14 and P21 in Tg21

and WT control mice, respectively. A timeline of postnatal development paired with an EPO-mediated quickening of mitochondrial progression in the hippocampus may optimize neuronal maturation, network formation, and, ultimately, cognitive function since most hippocampal synapses are formed and circuits established around this time. Indeed, we have observed greater glutamatergic and GABAergic synapses at P14 in Tg21 mice in previous research. The role of mitochondria in older and/or senescent adult neuronal tissue has been extensively investigated with regards to the biological causes and consequences of aging [63]. However, studies examining the role of mitochondrial function in the brain throughout postnatal development are few. Accordingly, these results provide novel insight into the mechanisms as to how EPO may improve cognition in early life. Our data suggests that EPO advances mitochondrial development in the hippocampus, which is observable by the second postnatal week of development versus the third week in WT control animals, and this influence on mitochondrial physiology may help confer a cognitive advantage later in life.

EPO overexpression improves cognition by early adulthood

Continued evidence shows that EPO enhances spatial memory across several models of disease [19,24,25,57]. Hippocampal CA1 principal cells have a well-defined role as cognition-relevant but hypoxia-vulnerable [64]. Mitochondrial function, especially as it pertains to the hippocampus, has also been shown to influence spatial memory throughout life [51,53]. Our paired observations of concentrated EpoR expression on CA1 cells and higher rates of cellular respiration in the hippocampus of Tg21 mice led us to speculate that EPO overexpression may also improve hippocampal-mediated cognition. Spatial memory and short-term memory were tested using the MWM and NOR tests,

respectively. Both tests showed improved memory in Tg21 mice. The MWM test showed significantly shorter escape latency during acquisition and reversal phases with reduced swim path length. These measures were all influence by the genotypic difference in task performance speed. We previously reported improved exercise performance in Tg21 mice with a longer time to exhaustion that was independent of systemic hematological differences (e.g. hematocrit) [65]. Perhaps the faster swim speed observed in the current study could be partially explained by diminished influence of central fatigue on physical function in Tg21 animals. It could be postulated, that EPO-induced improved metabolic control in the brain plays a critical role in limiting maximal exercise capacity [66]. Indeed higher mitochondrial content was observed in Tg21 mice, however, maximal coupled respiration, P_{CI+CII}, the respiratory state that best reflects *in vivo* oxidative phosphorylation potential, did not differ between WT controls and Tg21 mice at P60. Moreover, the shorter swim path length to find the platform, as demonstrated by Tg21 mice, suggests improved spatial orientation most likely attributed to enhanced synaptic number and plasticity as previously shown [6,9,67]. The NOR test with spatial cues examined the influence of EPO on short-term and long-term memory. Throughout the training phase, Tg21 mice showed increased activity but total exploration time was like WT controls. Ultimately, our findings suggest that EPO may improve short-term memory, as demonstrated by Tg21 mice compared to their WT counterparts, but long-term memory remained similar between genotypes. It is important to note that the NOR test is not exclusively hippocampal-dependent; NOR test performance also relies on cortical areas, such as the visual cortex, where EpoR expression was not present. The role of the hippocampus, cortex, and their integrated communication in developing short- and long-term memory is not fully

understood. However, the neural mechanisms used to establish short- and long-term memory are known to be somewhat independent [68]. While we cannot currently provide a clear description explaining the disparate influence of EPO on short- and long-term memory, our observations of Tg21 mice compared to their WT counterparts in NOR testing suggest a role of EPO to enhance short-term memory. Finally, T-maze working memory, which involves areas of the brain other than the hippocampus, showed no differences in spontaneous alternation between genotypes but Tg21 mice were faster in the choice, as in the other tests. This study's collective data set suggests that EPO-induced improved mitochondria number and function in the brain improves performance time and learning, and enhances spatial memory, most likely as an influence on synaptic number and plasticity into early adulthood.

General references about mitochondrial maturation in the brain throughout postnatal development

We have previously shown that mitochondrial respiration stimulated by NADH-linked mitochondrial respiration, analagous to P_{CI}, parallels the maturation of the cerebral cortex and brainstem when assessed at P3, P21, and adulthood [28]. Our current findings corroborate and build upon this data previously published by showing that the hippocampus and cerebral cortex show similar rates of NADH-linked respiration at P3, which then increase throughout postnatal development until they reach a peak at P21 in WT animals. However, NADH-linked respiration is higher in the brainstem at P3 when compared to hippocampal and cortical measures. This staggered bioenergetic maturation throughout postnatal development suggests that the brainstem develops and matures earlier than the hippocampus and cerebral cortex. Furthermore, these three separate

regions of the brain appear to share similar rates of respiration at P21, indicating that the energetic demand associated with neural maturation across the brain plateaus in WT animals around the age of weaning in mice.

Conclusion

This study reports evidence demonstrating that EPO overexpression in the CNS throughout postnatal development is associated with enhanced hippocampal dependent cognition. It appears that elevated concentrations of EPO preferentially act on CA1 pyramidal cells, as EpoR expression throughout postnatal development concentrates in this area. EPO signalling on the CA1 area increases p-Erk1/2 and p-Akt while hastening local mitochondrial maturation by approximately one week (~33% increase), which functionally increases oxidative potential through mitochondrial expansion without any evidence of concomitant oxidant strain in mitochondrial or cytosolic cellular compartments. Expedited mitochondrial development coincides with enhanced hippocampally dependent spatial memory. These findings highlight the clinical potential of EPO to maintain healthy hippocampal maturation and prevent neurodevelopmental delay after perinatal hypoxic-ischaemic injury.

METHODS

Animals

Mitochondrial analyses were conducted with both sexes using wild-type control (WT) and transgenic (Tg21) [35,69] mice at postnatal (P) ages: 3, 7; 14; 21, and 60 (n = 6-8). Behavioural tests were performed at early adulthood (P48-60). Tg21 hemizygous mice were backcrossed with C57Bl/6 mice more than ten generations to obtain the corresponding control mice and Tg21 mice were bred to homozygosity.

All mice were bred and housed under standard conditions at the University of Zurich. Animals were kept on a 12/12-h light/dark cycle with food and water provided *ad libitum*. Animal experiments were performed following the ARRIVE guidelines and were approved by the Cantonal Veterinary Office of Zurich, Switzerland (ZH177_16).

Blood samples for measures of hematocrit, hemoglobin and plasma EPO

Mice (P60) were anesthetized with a subcutaneous injection containing 100 mg/kg ketamine (Ketasol-100; Dr. Graub, Switzerland), 20 mg/kg xylazine (Rompun; Bayer, Germany), and 3 mg/kg acepromazine (Sedalin, Switzerland). Blood samples were taken by cardiac puncture with a 27 G needle attached to a 1 mL heparinized syringe. The blood was immediately transferred into an Eppendorf tube (1mL) to determine hematocrit, hemoglobin, and plasma EPO concentrations.

Duplicate measures of hematocrit were collected using micro capillary tubes (Micro hematocrit tube 100, Assistant) and immediately centrifuged (Hettich, Tuttlingen, Germany) for 5 min at 10 X 10^3 rpm (Autokit II, Pharmap, Geneva, Switzerland). Hemoglobin concentration was determined using Abbott Cell Dyn 3500 (Abbott Diagnostic Division, Santa Clara, CA, USA). Plasma EPO concentrations were assessed using a commercial kit (Epo-Trac 1251 RIA kit; DiaSorin, Saluggia, Italy) as previously described [70].

Statistical comparisons of hematocrit, hemoglobin, and plasma EPO between genotypes were each completed with a Student's t-test, (Prism 8.0.1. GraphPad Software, San Diego, CA, USA).

Measurement of mouse EPO (mEPO) and recombinant human EPO (rhEPO) in brain, kidney, liver, and spleen tissues

Concentrations of rhEPO were determined from frozen samples of brain, kidney, liver, and spleen from WT (P5) and Tg21 (both P5 and P21) mice using a commercial kit (Quantikine IVD ELISA, human erythropoietin, R&D Systems). Fresh wet weights of brain and spleen samples were registered for comparison. Main effects of genotype were identified with a 1-way ANOVA and post hoc analyses identifying individual group differences were conducted using Dunnett's test for multiple comparisons (GraphPad Prism 8.0.1.).

mEPO and rhEPO levels in the brain were additionally assessed at P60 in WT and Tg21 mice using commercial kits (Quantikine ELISA, mouse erythropoietin, and human erythropoietin, R&D systems).

Main effects of genotype between isoforms were determined using a 2-way ANOVA and post-hoc analyses identifying individual group differences were conducted with Sidak's correction for multiple comparisons (GraphPad Prism 8.0.1.).

Measurement of hippocampal EPO protein expression

Hippocampal EPO from WT and Tg21 mice was assessed in snap frozen samples throughout development using a radioimmunoassay (RIA) kit (Epo-Trac 1251 RIA kit; DiaSorin, Saluggia, Italy) as previously described [70].

Main effects of genotype and age were determined using a 2-way ANOVA and post hoc analyses identifying individual group differences were conducted with Sidak's correction for multiple comparisons (GraphPad Prism 8.0.1.).

EPO receptor (EpoR) mRNA expression in hippocampus and cortex

Hippocampal and cortical total RNA was isolated and purified (ReliaPrep RNA Miniprep System, Promega) from WT and Tg21 brain tissue at P3, P7, P14 and P21. RNA yield and purity were determined spectrophotometrically (Nanodrop 2000, Thermo Scientific). Total RNA yield was determined at 260 nm; purity was estimated by the relative absorbances at 260 and 280 (A_{260}/A_{280}). cDNA was obtained by reverse transcription.

Quantitative real time polymerase chain reaction (qRT-PCR) experiments were performed on a 7500 fast real-time PCR system (ThermoFisher Scientific, Waltham, MA, USA) using Select Master mix SYBR Green (Applied Biosystems). Primers for mouse EpoR mRNA: forward (5'-acaagggtaacttccagctgtg-3'), EpoR mRNA reverse (5'-gatcctcagggaaggagctg-3'), and internal control murine glyceraldehyde 3-phosphate dehydrogenase (GAPDH (mmu)) forward (5'-aatgtgtccgtcgtggatctg-3') and GAPDH (mmu) reverse (5'-catacttggcaggtttctccag-3) were designed with Primer 3.0. Software. Oligo properties were calculated using Oligo Analyzer 3.1 (IDT) Software. All samples were analyzed in duplicate. Relative quantifications were performed using the comparative Ct method. The fold change 2^(-ΔΔCT) values for each set of duplicates were averaged and normalized to mmu GAPDH. Each group of samples were normalized to WT P3 hippocampus. Main effects of genotype and age on EpoR mRNA expression were determined using a 2-way ANOVA and post hoc analyses identifying individual group differences were conducted with Sidak's correction for multiple comparisons (GraphPad Prism 8.0.1.).

Fluorescence in situ hybridization (FISH)

Tissue preparation

Postnatal WT and Tg21 male mice (P60), were deeply anesthetized with an intraperitoneal injection of sodium pentobarbital (50 mg/kg; Nembutal, Kantonsapotheke Zürich) followed by decapitation and dissection of brain tissue on ice. Hemispheres where then frozen on dry ice and stored at -80°C. Serial brain sections of 10 µm were cut using Leica Cryostat, mounted on Superfrost slides and stored at -80°C.

FISH

Murine EPO receptor (mEpoR) was identified using the RNAscope Multiplex Fluorescent Reagent Kit v2 (Advanced Cell Diagnostics) and fluorophore Opal 520 (Perkin Elmer). RNAscope 3-plex positive and negative control probes were always run in parallel.

At time of use, fresh frozen tissue was mounted on cryoslides (Super Frost Plus, Thermo Scientific Waltham, MA, USA) in a cryostat kept at -22°C. Slides were postfixed for 30 min at 4°C in 4% paraformaldehyde prepared in 0.15 M sodium phosphate buffer (pH 7.4), treated 10 min with hydrogenperoxide at room temperature, target retrieval for 10 min at 85°C (RNAscope Target Retrieval Reagent) and protease treatment with Protease Plus for 30 min at 40°C. Probes were hybridized for 2 h at 40°C. Slides were washed in Tris-Triton buffer, pH 7.4 followed by amplification steps (RNAscope Amp1-Amp3) and signal development (HRP-C1 + fluorophore 1). Lastly, slides were incubated for 3 min in DAPI counterstaining and cover slipped with mounting DAKO medium (DAKO Omnis).

FISH image analysis

Representative samples were imaged in a Zeiss LSM 700 confocal laser scanning microscope (Carl Zeiss AG, Oberkochen, Germany). Z-stack images (6 optical sections, 0.5 μm step size) were acquired at 40x magnification.

Western Blot analysis

Brain tissue samples were collected from WT and Tg21 mice at P3, P7, P14, P21, and P60. Animals were deeply anesthetized with an intraperitoneal injection of sodium pentobarbital (50 mg/kg; Nembutal, Kantonsapotheke Zürich) followed by decapitation and dissection of brain tissue on ice. Hippocampus and caudal cortex were dissected and placed on ice. Samples from each animal were independently processed (n=4 animals/group). Total hippocampal tissue was homogenized by transferring the tissue through a 21 G needle 5 times in ice cold 300 µl RIPA buffer (50 mM Tris/HCl pH 8.0, 150 mM NaCl, 1% NP-40, 0.5% Na deoxycholate, 1 mM EDTA, 0.1% SDS) with Protease Inhibitor Cocktail Set III, EDTA-Free diluted 1:100 (Merck Millipore, #539134), 1 mM Sodium orthovanadate, and 20 mM sodium fluoride as tyrosine and serine/threonine phosphatases inhibitors. Samples were kept on ice for 30 min and whole cell lysates were collected after centrifugation at 13000 rpm for 10 mins at 4 °C. Protein concentrations were determined using a Pierce BCA assay (Thermo Scientific, #23228, #23224). Loading samples (4x) were prepared by boiling at 70°C for 5 min in a Laemmli buffer (4% SDS, 20% glycerol, 10% mercaptoethanol, 0.004% bromophenol blue and 0.125 M Tris HCl pH 6.8). Protein samples (40 µg) were run in 10% (for AKT, phospho AKT, Erk1/2, phospho Erk1/2 and VDAC1 proteins) or 12.5% (for mitochondrial electron transport system proteins) SDS-PAGE gels (Bio-Rad, USA) for 90 min at 18 mA. Samples were then transferred for 1-2 h at 120 V to 0.45 µm nitrocellulose blotting membrane (GE

Healthcare, #10600002) using TE62 Transfer tank with cooling chamber (Hoefer™, USA). Membranes were washed 2x for 10 min with 0.05% TBST followed by blocking in 5% skimmed milk or bovine serum albumin (BSA) in 0.05% TBST for 1 h at room temperature. BSA was used for membrane blocking with phosphoprotein staining. Membranes were incubated at 4°C overnight with the following primary antibodies diluted 1:1000 in 5% skimmed milk or BSA in 0.05% TBST solution: rabbit anti-p44/42 MAPK (Erk1/2) (Cell Signalling, #9102); rabbit anti-Phospho-p44/42 MAPK (p-Erk1/2) (Cell signalling, #9101); mouse anti-AKT(pan) (Cell Signalling, #9272); 1:1000 rabbit anti-Phospho-AKT(Ser473) (Cell Signalling, #9271); rabbit anti-VDAC1/Porin antibody (abcam, #ab15895). Membranes were incubated at a 1:250 in OxPhos Rodent WB Antibody Cocktail (ThermoFisher Scientific, #458099), and rabbit anti-COX IV monoclonal antibody (3E11) (Cell Signaling, #4850). Membranes were washed and incubated in horseradish peroxidase-(HRP) conjugated secondary antibodies, goat anti-rabbit IgG (Merck, 12-348) and goat anti-mouse IgG (Santa Cruz, #2032), diluted 1:3000 in 5% milk in 0.05% TBST. Bands were visualized using Super Signal West Femto (Thermo Scientific, #34095) and developed with FUJIFILM Intelligent Darkbox Las-3000. Secondary antibody solutions conjugated to fluorescent molecules for two-color detection of AKT and phospho (p) AKT proteins (anti-mouse IRDye 680 LT red and anti-rabbit IRDye 800CW green, respectively), diluted 1:8000 in 5% BSA in 0.05% TBST blocking solution for 1 h at room temperature.

Protein loading was controlled with a mouse monoclonal antibody anti-β-actin (Sigma, #A5316) for AKT and OxPhos proteins or a rabbit anti-vinculin antibody (abcam, #155120) for Erk1/2 and VDAC1 proteins. Protein values were analyzed densitometrically

with ImageJ (NIH) software. Bands intensities were corrected with values determined on β-actin or vinculin blots and expressed as relative values compared to WT mice.
Detection and analysis of fluorescent bands were completed with the Li-COR Odyssey Plataform (Bioscences).

Main effects of genotype and age on protein expression were compared with a 2-way ANOVA and post hoc analyses identifying individual group differences were conducted with Sidak's correction for multiple comparisons. Student's t-test was used for object discrimination index (GraphPad Prism 8.0.1.).

High resolution respirometry

Tissue sampling

Hippocampal tissue samples were collected from WT and Tg21 animals at postnatal ages P3, 7, 14, 21, and 60. Samples were blotted dry, assessed for wet weight in a balance-controlled scale (Dual Range Analytical Balance, Mettler Toledo AG, Switzerland), maintaining constant relative humidity and hydration consistency for stability of measures, and immediately immersed in ice-cold respiration medium MiR05 (110 mM sucrose, 0.5 mM EGTA, 3 mM $MgCl_2*6H_2O$, 80 mM KCl, 60 mM K-lactobionate, 20 mM taurine, 10 mM KH_2P0_4, 20 mM HEPES, and 1 g/l bovine serum albumin, pH= 7.1) [71]. All chemicals were obtained from Sigma-Aldrich (Switzerland).

High-resolution respirometry

Mass-specific (pmol O_2 / s * mg ww) oxygen consumption rates (OCR) were collected using a high-resolution Oxygraph-2k respirometer (Oroboros, Innsbruck, Austria). Standardized instrumental calibrations were performed to correct for the back-diffusion of oxygen into the chamber from various internal components, leak from the exterior, oxygen

consumption by the chemical medium, and sensor oxygen consumption. All experiments were carried out in a hyperoxygenated environment (> 200 nmol/ml) to prevent any potential oxygen diffusion limitations and oxygen flux was resolved by software allowing nonlinear changes in the negative time derivative of the oxygen concentration signal (DatLab, Oroboros, Innsbruck, Austria). All measures were collected at 37°C in a respiration buffer MiR06 (MiR05 + 280 iU/ml catalase) with saponin (50 µg/ml) to facilitate cell membrane permeabilization [29]. All substrate, uncoupler, and inhibitor titrations described below were added in series (Fig. 3a).

Respiratory titration protocol

The respiration protocol used examines individual aspects of respiratory control by initiating a specific sequence of respiratory states. Here we analyzed various respiratory states representative of mitochondrial proton leak (L), maximal rates of coupled oxidative phosphorylation (P), and maximal rates of uncoupled respiration (E). Each respiratory state is specific to the substrate(s), uncoupler(s), and inhibitor(s) included in the respiration medium at any given time in addition to the protonmotive force and the relation of respiration to ATP production. L-state respiration, with kinetically saturating substrate and oxygen concentrations, represents uncoupled respiration due to proton leak and slippage across the inner mitochondrial membrane with a maximal protonmotive force in the absence of ATP production and is comparable to the classical definition of either state 2 or 4 respiration [72]. Mitochondrially-derived oxidant production is highest during L-state respiration [73,74]. P-state respiration, with kinetically saturating substrates, oxygen, and thermodynamically favorable adenylate concentrations to facilitate oxidative phosphorylation, represents respiratory rates that are well-coupled to ATP synthesis with

a high protonmotive force and are comparable to the classical definition of state 3 respiration [72]. E-state respiration, with kinetically saturating substrate and oxygen concentrations along with optimal exogenous protonophore provision, represents non-coupled respiratory rates independent of ATP synthesis with a collapsed protonmotive force. Respiratory analysis began with the collection of L-state respiration without exogenous adenylates (L_N) following the addition of malate (2 mM) and octanoylcarnitine (0.2 mM). P-state respiration driven by electron input from the electron transfer flavoprotein complex and mitochondrial complex I (P_{ETF+CI}) was initiated with the addition of ADP (5 mM). As the brain poorly oxidizes lipid substrates, P_{ETF+CI} can serve as an internal control of sample purity. Indeed, we found negligible changes in respiration between basal, L_N, and P_{ETF+CI} respiration (see result section). Accordingly, any reference of electron input from the electron transfer flavoprotein complex will be excluded from respiratory state identification throughout the results and discussion. P-state respiration with maximal electron input from mitochondrial complex I (P_{CI}) was induced following the additions of pyruvate (5 mM) and glutamate (10 mM). Maximal rates of P-state respiration, and the best representation of maximal oxidative phosphorylation potential *in vivo*, were then initiated with the addition of succinate (10 mM), which adds additional electron input from mitochondrial complex II (P_{CI+CII}). Maximal E-state respiration (E_{CI+CII}) was achieved with titrations of the protonophore, carbonyl cyanide p-(trifluoromethoxy) phenylhydrazone (FCCP), in 0.5 µM steps up to an optimum concentration (ranging from 1.5–3 µM). E-state respiration primarily reflecting electron input via mitochondrial complex II (E_{CII}) was then determined following the addition of rotenone (0.5 µM) and subsequent inhibition of mitochondrial complex I. Finally, non-mitochondrial residual oxygen

consumption (ROX) was induced with the addition of antimycin A (2.5 µM) and attendant inhibition of mitochondrial complex III. All respiratory states were corrected for measures of ROX. Upon completing respiratory state analyses, ascorbate (2 mM) and N,N,N',N'-tetramethyl-1,4-benzenediamine, dihydrochloride (TMPD, 500 µM) were simultaneously titrated into the chambers to assess cytochrome c oxidase (COX; complex IV) activity via mass-specific OCR (pmol O_2 / s * mg ww). Chemical calibrations were performed to determine and control for the auto-oxidation of TMPD occurring during measures of COX activity. For this, oxygen consumption is assessed over time using MiRO6 + saponin free of any biological sample with cytochrome c (10 µM), ascorbate (2 mM) and N,N,N',N'-tetramethyl-1,4-benzenediamine, dihydrochloride (TMPD, 500 µM) added to the chamber.

Mitochondria-specific respiration (%) was determined by normalizing mass-specific respiration (pmol O_2 / (s*mg ww) to COX activity (pmol O_2 / s * mg ww); (respiratory state respiration / COX activity) * 100. Main effects of genotype and age on mass-specific and mitochondria-specific respiratory rates were determined with a 2-way ANOVA and Bonferroni correction to control for type I error across multiple comparisons. The main effects and therefore the validity of our titration protocol, assessing general differences across respiratory states, were analyzed with a one-way repeated measures ANOVA and individual differences identified using Tukey's HSD post hoc test (GraphPad Prism 8.0.1.).

Assessment of cellular oxidative stress

Protein extraction

Samples were homogenized in phosphate buffer (PBS +EDTA), centrifuged 10 min at 12000 g, and the supernatant collected. This fraction was aliquoted and stored at -80°C

until analysis. Fractional protein concentrations were determined by a standard colorimetric BCA assay kit (Thermo Scientific, catalogue#23225) and all subsequent measurements were normalized to protein concentration.

NADPH oxidase (NOX) activity

NOX activity was calculated by measuring the kinetic of appearance of the complex superoxide anion/nitrotetrazolium blue (NTB) and adapted by Laouafa *et al* [75]. Briefly 20 µl of sample in duplicate was mixed with 250 µl of cocktail composed of nitroblue tetrazolium (NTB - 2.2 mM in water), Tris-HCL pH 8 (2.8 mM), diethylene-triamine-penta-acetic acid (1.3 mM in Tris-HCL), and 30 µl (100 µM/well) of fresh NADPH .solution (100 mM/well). The microplate was shaken 3 min at room temperature. Absorbance was assessed at 560 nm every 30 s for 5 min using a Synergy H1 Hybrid reader (BioTek). NOX activity was determined from the slope of formazan blue formation over time.

Cytosolic superoxide dismutase 1 (SOD1) activity

SOD1 activity was assessed in cytosolic fractions and determined by the reactionary inhibition between $O_2^{\cdot-}$ produced by a hypoxanthine-xanthine oxidase system and NTB. For this, the same cocktail described above for measures of NOX activities was used in duplicate with the addition of hypoxanthine (0.19 mM). A fresh solution of xanthine oxidase (XO; 1.02 units/mL) was prepared and then 20 µL of sample, 250 µl of cocktail, and 20 µL of XO were added to each well and mixed for 4-5 s at room temperature. The absorbance was immediately determined at 450 nm every 30 s for 5 min (Synergy H1 Hybrid reader, BioTek). Four wells were used as blanks for this assay, with 20 µL of PBS 1x rather than samples, and 1mM of NaCN was added in all the wells to inhibit SOD1. SOD1 activity was determined by the difference in slopes of formazan blue formation over

time and those constructed from our blanks.

Main effects of genotype on NOX, SOD1, and the ratio of NOX/SOD1 were determined with a one-way ANOVA and individual differences identified using Fisher's least significant difference (LSD) method for multiple comparisons post hoc analysis (GraphPad Prism 8.0.1.).

Cognitive Functions Tests

Morris Water Maze (MWM), to test hippocampal-dependent spatial learning and memory; novel object recognition (NOR) which combines spatial and visual memory; and T-maze testing of working memory, which is a complex function that involves storage, organization, and update of information and involves the prefrontal cortex [76] were all performed with male and female animals of both genotypes at postnatal ages P48 – 60. After weaning animals were housed in the testing room with room a 12 h light/dark inverted cycle and access to food and water ad libitum in standard laboratory conditions. Mice were controlled three times per week and handled once weekly to minimize handling-related stress that could impact performance in the task. Tests were performed during the dark phase under dimly lit conditions (12 lux). Animals were video-tracked at 4.2 Hz and 256 x 256 pixel spatial resolution using a Noldus EthoVision 1.96 system (Noldus Information Technology, Wageningen NL, www.noldus.com) throughout testing.

Morris Water Maze (MWM) test

The MWM, test to test hippocampal mediated spatial-memory, was employed as previously described [77]. The circular black arena was 150 cm in diameter with a wall height of 50 cm. High contrast spatial cues were placed on walls of the encompassing room and inside the arena above the water surface. The arena was filled with water to a

height of 15 cm and maintained at 25°C. Day 1 consisted of teaching the mice to identify the escapable end point of the task by training them to find a visible Plexiglas platform (16 x 16 cm) placed randomly 0.5 cm underneath the water surface. Days 2-5 consisted of training the animals to find the hidden platform, which remained in a fixed position (acquisition phase). Throughout the acquisition phase the water was made opaque by the addition of milk and the target platform was hidden 0.5 cm underneath the water surface 35 cm away from the surrounding walls in one quadrant (NW, NE, SE or SW). Animals performed 6 trials of 120 s per day, with an inter-trial interval (ITI) of 30 min. On day 6 the platform was moved to the opposite quadrant (reversal phase) and four trials of 120 min were registered to measure spatial retention. The swim pathway of each mouse was automatically tracked and the time to reach the platform (escape time), total swim distance (m) and speed (m/s) were calculated.

Novel Object Recognition (NOR) test

The NOR test relies on the animal's intrinsic preference for novelty. The choice to explore a novel object reflects learning and recognition memory, which also involves the hippocampus [78,79] together with cortical areas such as the visual cortex.

Mice were first habituated to an open field-testing arena (60 x 60 x 50 cm) with two spatial environmental cues on the walls for 10 min on two consecutive days. Mice were free to explore during habituation and the total activity time was registered. On the third day, animals were allowed 5 min to explore two equal objects placed in specific quadrants of the arena. The mice were subsequently removed from the arena for 1h ITI. One of the objects was replaced by another object similar in height and volume but different in shape and texture. Following this brief ITI, mice were reintroduced to the testing arena and

allowed to freely explore the new object for 5 min. The next day (ITI of 24 h), mice were again allowed to explore the open testing field in the presence of a familiar and another new object. Time spent exploring each object and number of explorations were recorded. Object discrimination ratio was calculated by: TN / (TN + TF). TN = time exploring the new object, TF = time exploring the familiar object. Animals that explored each object less than 10 s were excluded from the test.

T- Maze working memory test

Working-memory was assessed by a discrete-trial rewarded-alternation task in a T-maze made of grey poly-vinyl-chloride/plexiglas (each arm measures 30x10 cm) with a removable central partition and one guillotine door for each arm of the maze for further details see [80]. Each mouse was habituated to testing and performed 6 trials over two consecutive days. One trial consisted of two successive runs through the maze. In the first run (forced run) both arms were available and in one arm is a food reward (R). Once the animal entered the sample arm and consumed the R, the door was lowered and they were retained in the sample arm for 30 s. Mice were then immediately returned to the start arm for the second run in which both arms were now available, so the animals could enter either arm (choice run), however, food was available only in the arm not entered on the first run. Consequently, working memory is necessary to remember which arm was the sample arm in the first trial and to alternate. A run was terminated if a choice was not made within 2 min. The sample arm available to the mice on the first forced run varied randomly from trial to trial. Following each trial, the mice were removed from the T-maze and returned to their cage for a 1 h ITI. The working-memory component of this task is

quantified by the spontaneous alternation in choosing different arms between trial runs. Percentage of alternation and time to reach the reward was calculated per animal.

The main effects of genotype for outcome variables derived from MWM and NOR tests were analyzed using a 1-way ANOVA and post hoc analyses identifying individual group differences were conducted with Sidak's correction for multiple comparisons. A student's t-test was used to compare T-maze spontaneous alteration between genotypes (GraphPad Prism 8.0.1.).

For all statistical evaluations included in this study, unless otherwise specified, an α of

$p < .05$ was considered significant and data are reported as mean ± SD.

REFERENCES

1 Marti, H. H. *et al.* Erythropoietin gene expression in human, monkey and murine brain. *Eur J Neurosci* **8**, 666-676 (1996).

2 Brines, M. & Cerami, A. Emerging biological roles for erythropoietin in the nervous system. *Nat Rev Neurosci* **6**, 484-494, doi:10.1038/nrn1687 (2005).

3 Dey, S. *et al.* Sex-specific brain erythropoietin regulation of mouse metabolism and hypothalamic inflammation. *JCI Insight* **5**, doi:10.1172/jci.insight.134061 (2020).

4 Othman, M. A. M. *et al.* Erythropoietin Protects Against Cognitive Impairment and Hippocampal Neurodegeneration in Diabetic Mice. *Behav Sci (Basel)* **9**, doi:10.3390/bs9010004 (2018).

5 Gonzalez, F. F. *et al.* Erythropoietin sustains cognitive function and brain volume after neonatal stroke. *Dev Neurosci* **31**, 403-411, doi:10.1159/000232558 (2009).

6 Kumral, A. *et al.* Erythropoietin in neonatal brain protection: the past, the present and the future. *Brain Dev* **33**, 632-643, doi:10.1016/j.braindev.2010.10.014 (2011).

7 Miskowiak, K., O'Sullivan, U. & Harmer, C. J. Erythropoietin enhances hippocampal response during memory retrieval in humans. *J Neurosci* **27**, 2788-2792, doi:10.1523/JNEUROSCI.5013-06.2007 (2007).

8 Hassouna, I. *et al.* Revisiting adult neurogenesis and the role of erythropoietin for neuronal and oligodendroglial differentiation in the hippocampus. *Mol Psychiatry* **21**, 1752-1767, doi:10.1038/mp.2015.212 (2016).

9 Dias, R. B. *et al.* Erythropoietin Induces Homeostatic Plasticity at Hippocampal Synapses. *Cereb Cortex* **28**, 2795-2809, doi:10.1093/cercor/bhx159 (2018).

10 Ransome, M. I. & Turnley, A. M. Systemically delivered Erythropoietin transiently enhances adult hippocampal neurogenesis. *J Neurochem* **102**, 1953-1965, doi:10.1111/j.1471-4159.2007.04684.x (2007).

11 Dmytriyeva, O. *et al.* Short erythropoietin-derived peptide enhances memory, improves long-term potentiation, and counteracts amyloid beta-induced pathology. *Neurobiology of aging* **81**, 88-101, doi:10.1016/j.neurobiolaging.2019.05.003 (2019).

12 Esmaeili Tazangi, P., Moosavi, S. M., Shabani, M. & Haghani, M. Erythropoietin improves synaptic plasticity and memory deficits by decrease of the neurotransmitter release probability in the rat model of Alzheimer's disease. *Pharmacology, biochemistry, and behavior* **130**, 15-21, doi:10.1016/j.pbb.2014.12.011 (2015).

13 Ehrenreich, H. *et al.* Exploring recombinant human erythropoietin in chronic progressive multiple sclerosis. *Brain* **130**, 2577-2588, doi:10.1093/brain/awm203 (2007).

14 Juul, S. E. & Pet, G. C. Erythropoietin and Neonatal Neuroprotection. *Clin Perinatol* **42**, 469-481, doi:10.1016/j.clp.2015.04.004 (2015).

15 Rangarajan, V. & Juul, S. E. Erythropoietin: emerging role of erythropoietin in neonatal neuroprotection. *Pediatr Neurol* **51**, 481-488, doi:10.1016/j.pediatrneurol.2014.06.008 (2014).

16 Juul, S. E., Mayock, D. E., Comstock, B. A. & Heagerty, P. J. Neuroprotective potential of erythropoietin in neonates; design of a randomized trial. *Matern Health Neonatol Perinatol* **1**, 27, doi:10.1186/s40748-015-0028-z (2015).

17 McPherson, R. J. & Juul, S. E. Erythropoietin for infants with hypoxic-ischemic encephalopathy. *Current opinion in pediatrics* **22**, 139-145, doi:10.1097/MOP.0b013e328336eb57 (2010).

18 Xavier, J. M., Rodrigues, C. M. & Sola, S. Mitochondria: Major Regulators of Neural Development. *The Neuroscientist : a review journal bringing neurobiology, neurology and psychiatry* **22**, 346-358, doi:10.1177/1073858415585472 (2016).

19 Hara, Y. *et al.* Presynaptic mitochondrial morphology in monkey prefrontal cortex correlates with working memory and is improved with estrogen treatment. *Proc Natl Acad Sci U S A* **111**, 486-491, doi:10.1073/pnas.1311310110 (2014).

20 Picard, M. & McEwen, B. S. Mitochondria impact brain function and cognition. *Proceedings of the National Academy of Sciences of the United States of America* **111**, 7-8, doi:10.1073/pnas.1321881111 (2014).

21 Millet, A. *et al.* Erythropoietin and Its Derivates Modulate Mitochondrial Dysfunction after Diffuse Traumatic Brain Injury. *Journal of neurotrauma* **33**, 1625-1633, doi:10.1089/neu.2015.4160 (2016).

22 Xiong, Y., Chopp, M. & Lee, C. P. Erythropoietin improves brain mitochondrial function in rats after traumatic brain injury. *Neurological research* **31**, 496-502, doi:10.1179/174313208X353703 (2009).

23 Laouafa, S. *et al.* Erythropoietin and caffeine exert similar protective impact against neonatal intermittent hypoxia: Apnea of prematurity and sex dimorphism. *Experimental neurology* **320**, 112985, doi:10.1016/j.expneurol.2019.112985 (2019).

24 Singhal, N. K. *et al.* Erythropoietin Upregulates Brain Hemoglobin Expression and Supports Neuronal Mitochondrial Activity. *Mol Neurobiol* **55**, 8051-8058, doi:10.1007/s12035-018-0971-6 (2018).

25 Horng, L. Y. *et al.* Activating mitochondrial function and haemoglobin expression with EH-201, an inducer of erythropoietin in neuronal cells, reverses memory impairment. *Br J Pharmacol* **172**, 4741-4756, doi:10.1111/bph.13248 (2015).

26 Al-Qahtani, J. M., Abdel-Wahab, B. A. & Abd El-Aziz, S. M. Long-term moderate dose exogenous erythropoietin treatment protects from intermittent hypoxia-induced spatial learning deficits and hippocampal oxidative stress in young rats. *Neurochemical research* **39**, 161-171, doi:10.1007/s11064-013-1201-2 (2014).

27 Dayyat, E. A., Zhang, S. X., Wang, Y., Cheng, Z. J. & Gozal, D. Exogenous erythropoietin administration attenuates intermittent hypoxia-induced cognitive

deficits in a murine model of sleep apnea. *BMC neuroscience* **13**, 77, doi:10.1186/1471-2202-13-77 (2012).

28 Arias-Reyes, C., Losantos-Ramos, K., Gonzales, M., Furrer, D. & Soliz, J. NADH-linked mitochondrial respiration in the developing mouse brain is sex-, age- and tissue-dependent. *Respir Physiol Neurobiol* **266**, 156-162, doi:10.1016/j.resp.2019.05.011 (2019).

29 Herbst, E. A. & Holloway, G. P. Permeabilization of brain tissue in situ enables multiregion analysis of mitochondrial function in a single mouse brain. *J Physiol* **593**, 787-801, doi:10.1113/jphysiol.2014.285379 (2015).

30 Herbst, E. A. F., George, M. A. J., Brebner, K., Holloway, G. P. & Kane, D. A. Lactate is oxidized outside of the mitochondrial matrix in rodent brain. *Appl Physiol Nutr Metab* **43**, 467-474, doi:10.1139/apnm-2017-0450 (2018).

31 Dias, C., Lourenco, C. F., Barbosa, R. M., Laranjinha, J. & Ledo, A. Analysis of respiratory capacity in brain tissue preparations: high-resolution respirometry for intact hippocampal slices. *Anal Biochem* **551**, 43-50, doi:10.1016/j.ab.2018.05.010 (2018).

32 Kanterewicz, B. I., Knapp, L. T. & Klann, E. Stimulation of p42 and p44 mitogen-activated protein kinases by reactive oxygen species and nitric oxide in hippocampus. *J Neurochem* **70**, 1009-1016, doi:10.1046/j.1471-4159.1998.70031009.x (1998).

33 Kishida, K. T., Pao, M., Holland, S. M. & Klann, E. NADPH oxidase is required for NMDA receptor-dependent activation of ERK in hippocampal area CA1. *J Neurochem* **94**, 299-306, doi:10.1111/j.1471-4159.2005.03189.x (2005).

34 Monge Naldi, A. *et al.* Neuronal erythropoietin overexpression protects mice against age-related hearing loss (presbycusis). *Neurobiol Aging* **36**, 3278-3287, doi:10.1016/j.neurobiolaging.2015.08.015 (2015).

35 Wiessner, C. *et al.* Increased cerebral infarct volumes in polyglobulic mice overexpressing erythropoietin. *J Cereb Blood Flow Metab* **21**, 857-864, doi:10.1097/00004647-200107000-00011 (2001).

36 Becker, V. *et al.* Covering a broad dynamic range: information processing at the erythropoietin receptor. *Science* **328**, 1404-1408, doi:10.1126/science.1184913 (2010).

37 Pokorny, J. & Yamamoto, T. Postnatal ontogenesis of hippocampal CA1 area in rats. I. Development of dendritic arborisation in pyramidal neurons. *Brain Res Bull* **7**, 113-120, doi:10.1016/0361-9230(81)90075-7 (1981).

38 Danglot, L., Triller, A. & Marty, S. The development of hippocampal interneurons in rodents. *Hippocampus* **16**, 1032-1060, doi:10.1002/hipo.20225 (2006).

39 Gomez-Di Cesare, C. M., Smith, K. L., Rice, F. L. & Swann, J. W. Axonal remodeling during postnatal maturation of CA3 hippocampal pyramidal neurons. *J Comp Neurol* **384**, 165-180 (1997).

40 Levin, S. & Godukhin, O. Developmental changes in hyperexcitability of CA1 pyramidal neurons induced by repeated brief episodes of hypoxia in the rat hippocampal slices. *Neurosci Lett* **377**, 20-24, doi:10.1016/j.neulet.2004.11.057 (2005).

41 Bao, H. *et al.* Protein kinase B (c-Akt), phosphatidylinositol 3-kinase, and STAT5 are activated by erythropoietin (EPO) in HCD57 erythroid cells but are

constitutively active in an EPO-independent, apoptosis-resistant subclone (HCD57-SREI cells). *Blood* **93**, 3757-3773 (1999).

42 Dudek, H. *et al.* Regulation of neuronal survival by the serine-threonine protein kinase Akt. *Science* **275**, 661-665, doi:10.1126/science.275.5300.661 (1997).

43 Franke, T. F., Kaplan, D. R. & Cantley, L. C. PI3K: downstream AKTion blocks apoptosis. *Cell* **88**, 435-437, doi:10.1016/s0092-8674(00)81883-8 (1997).

44 Siren, A. L. *et al.* Erythropoietin prevents neuronal apoptosis after cerebral ischemia and metabolic stress. *Proc Natl Acad Sci U S A* **98**, 4044-4049, doi:10.1073/pnas.051606598 (2001).

45 Li, Z., Theus, M. H. & Wei, L. Role of ERK 1/2 signaling in neuronal differentiation of cultured embryonic stem cells. *Dev Growth Differ* **48**, 513-523, doi:10.1111/j.1440-169X.2006.00889.x (2006).

46 Karpova, A., Sanna, P. P. & Behnisch, T. Involvement of multiple phosphatidylinositol 3-kinase-dependent pathways in the persistence of late-phase long term potentiation expression. *Neuroscience* **137**, 833-841, doi:10.1016/j.neuroscience.2005.10.012 (2006).

47 Raymond, C. R. LTP forms 1, 2 and 3: different mechanisms for the "long" in long-term potentiation. *Trends Neurosci* **30**, 167-175, doi:10.1016/j.tins.2007.01.007 (2007).

48 Adamcio, B. *et al.* Erythropoietin enhances hippocampal long-term potentiation and memory. *BMC Biol* **6**, 37, doi:10.1186/1741-7007-6-37 (2008).

49 Alonso, M. *et al.* Mitochondrial extracellular signal-regulated kinases 1/2 (ERK1/2) are modulated during brain development. *J Neurochem* **89**, 248-256, doi:10.1111/j.1471-4159.2004.02323.x (2004).

50 Accardi, M. V. *et al.* Mitochondrial reactive oxygen species regulate the strength of inhibitory GABA-mediated synaptic transmission. *Nat Commun* **5**, 3168, doi:10.1038/ncomms4168 (2014).

51 Liu, J. *et al.* Memory loss in old rats is associated with brain mitochondrial decay and RNA/DNA oxidation: partial reversal by feeding acetyl-L-carnitine and/or R-alpha -lipoic acid. *Proc Natl Acad Sci U S A* **99**, 2356-2361, doi:10.1073/pnas.261709299 (2002).

52 Tveden-Nyborg, P. *et al.* Vitamin C deficiency in early postnatal life impairs spatial memory and reduces the number of hippocampal neurons in guinea pigs. *Am J Clin Nutr* **90**, 540-546, doi:10.3945/ajcn.2009.27954 (2009).

53 McManus, M. J., Murphy, M. P. & Franklin, J. L. The mitochondria-targeted antioxidant MitoQ prevents loss of spatial memory retention and early neuropathology in a transgenic mouse model of Alzheimer's disease. *J Neurosci* **31**, 15703-15715, doi:10.1523/JNEUROSCI.0552-11.2011 (2011).

54 Mattson, M. P., Gleichmann, M. & Cheng, A. Mitochondria in neuroplasticity and neurological disorders. *Neuron* **60**, 748-766, doi:10.1016/j.neuron.2008.10.010 (2008).

55 Sheng, Z. H. & Cai, Q. Mitochondrial transport in neurons: impact on synaptic homeostasis and neurodegeneration. *Nat Rev Neurosci* **13**, 77-93, doi:10.1038/nrn3156 (2012).

56 Hebert-Chatelain, E. *et al.* A cannabinoid link between mitochondria and memory. *Nature* **539**, 555-559, doi:10.1038/nature20127 (2016).

57 Almaguer-Melian, W. *et al.* Erythropoietin Promotes Neural Plasticity and Spatial Memory Recovery in Fimbria-Fornix-Lesioned Rats. *Neurorehabil Neural Repair* **29**, 979-988, doi:10.1177/1545968315572389 (2015).

58 Wang, L. *et al.* PPARalpha and Sirt1 mediate erythropoietin action in increasing metabolic activity and browning of white adipocytes to protect against obesity and metabolic disorders. *Diabetes* **62**, 4122-4131, doi:10.2337/db13-0518 (2013).

59 Carraway, M. S. *et al.* Erythropoietin activates mitochondrial biogenesis and couples red cell mass to mitochondrial mass in the heart. *Circ Res* **106**, 1722-1730, doi:10.1161/CIRCRESAHA.109.214353 (2010).

60 Wang, L. *et al.* Erythropoietin contributes to slow oxidative muscle fiber specification via PGC-1alpha and AMPK activation. *Int J Biochem Cell Biol* **45**, 1155-1164, doi:10.1016/j.biocel.2013.03.007 (2013).

61 Plenge, U. *et al.* Erythropoietin treatment enhances muscle mitochondrial capacity in humans. *Front Physiol* **3**, 50, doi:10.3389/fphys.2012.00050 (2012).

62 Wang, L., Di, L. & Noguchi, C. T. Erythropoietin, a novel versatile player regulating energy metabolism beyond the erythroid system. *Int J Biol Sci* **10**, 921-939, doi:10.7150/ijbs.9518 (2014).

63 Gaignard, P. *et al.* Role of Sex Hormones on Brain Mitochondrial Function, with Special Reference to Aging and Neurodegenerative Diseases. *Front Aging Neurosci* **9**, 406, doi:10.3389/fnagi.2017.00406 (2017).

64 Schmidt-Kastner, R. Genomic approach to selective vulnerability of the hippocampus in brain ischemia-hypoxia. *Neuroscience* **309**, 259-279, doi:10.1016/j.neuroscience.2015.08.034 (2015).

65 Schuler, B. *et al.* Acute and chronic elevation of erythropoietin in the brain improves exercise performance in mice without inducing erythropoiesis. *FASEB J* **26**, 3884-3890, doi:10.1096/fj.11-191197 (2012).

66 Dalsgaard, M. K. & Secher, N. H. The brain at work: a cerebral metabolic manifestation of central fatigue? *J Neurosci Res* **85**, 3334-3339, doi:10.1002/jnr.21274 (2007).

67 Ehrenreich, H., Bartels, C., Sargin, D., Stawicki, S. & Krampe, H. Recombinant human erythropoietin in the treatment of human brain disease: focus on cognition. *J Ren Nutr* **18**, 146-153, doi:10.1053/j.jrn.2007.10.029 (2008).

68 Izquierdo, I., Medina, J. H., Vianna, M. R., Izquierdo, L. A. & Barros, D. M. Separate mechanisms for short- and long-term memory. *Behav Brain Res* **103**, 1-11, doi:10.1016/s0166-4328(99)00036-4 (1999).

69 Ruschitzka, F. T. *et al.* Nitric oxide prevents cardiovascular disease and determines survival in polyglobulic mice overexpressing erythropoietin. *Proc Natl Acad Sci U S A* **97**, 11609-11613, doi:10.1073/pnas.97.21.11609 (2000).

70 Glaus, T. M., Grenacher, B., Koch, D., Reiner, B. & Gassmann, M. High altitude training of dogs results in elevated erythropoietin and endothelin-1 serum levels. *Comp Biochem Physiol A Mol Integr Physiol* **138**, 355-361, doi:10.1016/j.cbpb.2004.05.008 (2004).

71 Jacobs, R. A. *et al.* Improvements in exercise performance with high-intensity interval training coincide with an increase in skeletal muscle mitochondrial content and function. *J Appl Physiol (1985)* **115**, 785-793, doi:10.1152/japplphysiol.00445.2013 (2013).

72 Chance, B. & Williams, G. R. The respiratory chain and oxidative phosphorylation. *Adv Enzymol Relat Subj Biochem* **17**, 65-134, doi:10.1002/9780470122624.ch2 (1956).

73 Barja, G. Mitochondrial oxygen radical generation and leak: sites of production in states 4 and 3, organ specificity, and relation to aging and longevity. *J Bioenerg Biomembr* **31**, 347-366, doi:10.1023/a:1005427919188 (1999).

74 Sanz, A. *et al.* Dietary restriction at old age lowers mitochondrial oxygen radical production and leak at complex I and oxidative DNA damage in rat brain. *J Bioenerg Biomembr* **37**, 83-90, doi:10.1007/s10863-005-4131-0 (2005).

75 Laouafa, S. *et al.* Estradiol Protects Against Cardiorespiratory Dysfunctions and Oxidative Stress in Intermittent Hypoxia. *Sleep* **40**, doi:10.1093/sleep/zsx104 (2017).

76 Goldman-Rakic, P. S. Cellular basis of working memory. *Neuron* **14**, 477-485, doi:10.1016/0896-6273(95)90304-6 (1995).

77 Bromley-Brits, K., Deng, Y. & Song, W. Morris water maze test for learning and memory deficits in Alzheimer's disease model mice. *J Vis Exp*, doi:10.3791/2920 (2011).

78 Squire, L. R., Wixted, J. T. & Clark, R. E. Recognition memory and the medial temporal lobe: a new perspective. *Nature reviews. Neuroscience* **8**, 872-883, doi:10.1038/nrn2154 (2007).

79 Broadbent, N. J., Gaskin, S., Squire, L. R. & Clark, R. E. Object recognition memory and the rodent hippocampus. *Learn Mem* **17**, 5-11, doi:10.1101/lm.1650110 (2010).

80 Deacon, R. M. & Rawlins, J. N. T-maze alternation in the rodent. *Nat Protoc* **1**, 7-12, doi:nprot.2006.2 [pii]10.1038/nprot.2006.2 (2006).

Acknowledgments

This work was supported by the University of Zürich, the Baugenossenschaft Zurlinden and the Swiss National Science Foundation by the MHV Grant PMPDP3_145480 to E.M.S.G. J.S. is supported by the “Fonds de recherché du Quebec-Santé” (FRQ-S; FQ121919). We kindly acknowledge Prof. Jean-Marc Fritschy for his scientific feedback and proof reading as well as Nicole Kachappilly, Dr. Tatjana Haenggi and Cornelia Schwerdel for excellent technical support.

Author contributions

E.M.S.G. designed the study; C.K-H., C.A-R., S.L. R.A.J., M.A.A., and E.M.S.G. performed research and data analyses; M.T., R.A.J., and J.S. provided expertise with mitochondria measurements and intellectual input; E.M.S.G and R.A.J. wrote the manuscript; M.G. provided the Tg21 mice, its expertise, and supported to conduct this project; and E.M.G.S., R.A.J., M.A.A., C.A-R., S.L., C.K-H., M.T., J.S., and M.G. approved the manuscript.

Competing interest

Authors have no conflict of interest to declare.

FIGURE LEGENDS

Figure 1. Overexpression of rhEPO in Tg21 mice is primarily restricted to the brain while EpoR expression in WT controls and Tg21 mice increase similarly throughout postnatal development but only in the hippocampus. a) Measures of spleen weight (mg-ww), hematocrit (%), hemoglobin (g/dL) and plasma EPO concentration (pg/ml) at P60, showing no differences between genotypes. Student's t-test analyses; $p = 0.33$, spleen; $p = 0.16$, hematocrit; $p = 0.20$ hemoglobin; and $p = 0.1$, plasma EPO. **b)** Protein expression of mouse EPO (mEPO) and rhEPO in the hippocampus at P60. Negligible expression of brain mEPO is detected in either genotype whereas rhEPO expression is significantly greater in Tg21 mice. 2-way ANOVA, $F(1,14) = 342$, $^{****}p < 0.0001$. **c)** Measures of rhEPO in brain, kidney, liver, and spleen in WT and Tg21 animals at P5 and in Tg21 at P21. rhEPO overexpression is primarily isolated to the brain, with a slight (~16% of respective measure in the brain) and transient expression in the liver of Tg21 mice at P5. 1-way ANOVA, $F(2,9) = 0.8$, $^{*}p = 0.048$. **d)** Total EPO protein expression (murine and recombinant human) across postnatal ages P: 1, 3, 7, 14, 21 and 90. EPO is greatly overexpressed in the hippocampus of Tg21 mice throughout postnatal development, decaying to its lowest difference (4-fold increase) respective to age-matched WT controls in adulthood (P90). 2-way ANOVA, $F(1,91) = 9613$, $^{****}p < 0.0001$. **e)** EpoR mRNA expression in the hippocampus of WT and Tg21 mice across postnatal ages P: 3, 7, 14 and 21. An age-induced increase in EpoR is shown with no difference between genotypes. 2-way ANOVA, $F(3,47) = 2.767$, $p = 0.10$. **f)** EpoR mRNA expression in the cortex of WT and Tg21 mice across postnatal ages P: 3, 7, 14 and 21. Primarily there is no change in EpoR expression with age or between genotypes. However, we did

observe a transient increase in WT mice at P14. 2-way ANOVA, F(3,47) = 18.14, ****p < 0.0001. **g)** Representative images of hippocampal (HPC) CA1 area and cortical L5-6 area (CTX) from young adult (P60) WT mice. EpoR mRNA expression is highly visible in HPC principal neurons whereas negligible EpoR mRNA can be seen in CTX. Scale: 20 μm.

Figure 2. EPO overexpression in the central nervous system (CNS) activates Erk1/2 and AKT in the hippocampus. a) Representative images of total Erk1/2 protein expression across postnatal ages P: 3, 7, 14 and 21 in WT and Tg21 mice and vinculin loading control. **b)** Quantification of total Erk1/2 protein shows no change throughout development or between genotypes. 2-way ANOVA, F(3,24) = 0.309, p = 0.583. **c)** Phosphorylated (p-)Erk1/2 protein expression across postnatal ages P: 3, 7, 14 and 21 in WT and Tg21 mice. **d)** Quantification of p-Erk1/2 shows highest levels of phosphorylation at P3 and P21 in both genotypes and 2-fold higher activation in the Tg21 mice across all measured ages. 2-way ANOVA, F(3,24) = 26.97, ****p < 0.0001. Multiple comparison: *, **, ***, ****: p<;0.05, p<0.01, p<;0.001, p<0.0001. **e)** Representative images of total AKT protein expression with β-actin loading control (red; top) and p-AKT (green) superimposed over total AKT (bottom) in WT and Tg21 mice at postnatal ages P: 3, 7, 14, and 21. **f)** Quantification of total AKT shows no change throughout development or difference between genotypes. 2-way ANOVA, F(3,24) = 1.347, p = 0.263. **g)** Quantification of p-AKT shows the lowest levels of phosphorylation in WT mice at P3 and higher values in Tg21 mice at P3 (5-fold), P7 (3-fold), P14 (3-fold) and P21 (3-fold). 2-way ANOVA, F(3,24) = 65.64, ****p < 0.0001, multiple comparisons: *, **, p<;0.05, p<0.01.

Figure 3. CNS EPO overexpression influences mass-specific respiratory control in postnatal hippocampus. a) Schematic representation of respirometric traces from a WT (top) and Tg21 (bottom) recording, which illustrate the change in oxygen concentration (nmol·ml^{-1}, left y-axis, blue line) and oxygen flux per mass (pmol O_2 / s * mg ww, right y-axis, red line) in hippocampal tissue at P21. Respiratory states were achieved through the titration of various substrates, inhibitors, as well as a protonophore. The order of respiratory state analysis from beginning to end (left-to-right) with the respective substrates, inhibitors, or protonophores added, as fully explained in the methods, consisted of: leak without adenylates (L_N, malate and octanoylcarnitine); coupled respiration with maximal electron input from mitochondrial complex I (P_{CI}, pyruvate and glutamate); maximal rates of coupled respiration with electron input from complex I and II (P_{CI+CII}, succinate); maximal noncoupled respiration (E) with electron input from complex I and II (E_{CI+CII}, steps of carbonyl cyanide p-trifluoromethoxy phenylhydrazone, FCCP, addition until respiration ceases to increase); noncoupled respiration with maximal electron input from mitochondrial complex II (E_{CII}, rotenone); and non-mitochondrial residual oxygen consumption (ROX, antimycin A). Following respiratory state analysis, ascorbate and N,N,N',N'-tetramethyl-1,4-benzenediamine, dihydrochloride (TMPD) were simultaneously added to assess cytochrome c oxidase (COX; complex IV) activity via mass-specific oxygen consumption rates (pmol O_2 / s * mg ww). **b)** Hippocampal mass-specific oxygen consumption rates (OCR) from WT (left) and Tg21 (right) mice at postnatal ages of P: 3, 7, 14, 21, and 60. L_N: 2-way ANOVA, $F(1,66) = 0.08$, $p = 0.78$; P_{CI}: 2-way ANOVA, $F(1,66) = 15.74$, $^{***}p = 0.0002$; P_{CI+CII}: 2-way ANOVA, $F(1,67) = 9.072$, $^{**}p = 0.0037$; and E_{CI+CII} 2-way ANOVA, $F(1,66) = 21.59$, $^{****}p < 0.0001$. **c)** P_{CI} respiration,

d) P_{CI+CII} respiration, and **e)** E_{CI+CII} respiration comparisons throughout postnatal development in WT vs Tg21 mice. Tg21 mice displayed higher rates of P_{CI} at P14 and P21, P_{CI+CII} at P21, and E_{CI+CII} respiration at P14 and P21. Multiple comparisons c-e: **, ***, ****: $p < 0.01$, $p < 0.001$, and $p < 0.0001$.

Figure 4. CNS EPO overexpression does not influence respiration when normalized to a biomarker of mitochondrial content in postnatal hippocampus. a) Cytochrome C oxidase activity (COX, pmol O_2 / s * mg ww) in the hippocampus of WT and Tg21 throughout postnatal development. Tg21 mice show higher COX activity at P14, P21, and P60. 2-way ANOVA, $F(1,66) = 27.32$, ****$p < 0.0001$. Multiple comparisons: *, **: $p < 0.05$, and $p < 0.01$. **b)** Mass-specific oxygen consumption rates (OCR) relative to COX (%) in WT and Tg21 mice for leak respiration without adenylates (L_N); coupled respiration with maximal electron input from mitochondrial complex I (P_{CI}); maximal rates of coupled respiration with electron input from complex I and II (P_{CI+CII}); and maximal noncoupled respiration with electron input from complex I and II (E_{CI+CII}). Mass-specific respiratory differences between genotypes are lost when normalizing to COX, a surrogate of mitochondrial content. **c)** Correlations between mitochondrial content via COX activity and mito-specific respiration for P_{CI} and **d)** P_{CI+CII} throughout postnatal development in WT (left panels) and Tg21 (right panels) mice, respectively. An increase in respiration throughout postnatal development is observed along with an increase in mitochondrial content in both genotypes for both respiratory states. Mitochondrial content is greater in at P21 and P60 in WT mice, and at P14, P21 and P60 in Tg21 mice.

Figure 5. CNS EPO overexpression increases additional evidence of mitochondrial content in hippocampus throughout postnatal development. Representative images of: **a)** total voltage-dependent anion channel 1 (VDAC1) across postnatal ages P: 3, 7, 14 and 21 against vinculin loading control; and **c)** mitochondrial electron transport complex protein expressions across postnatal ages P: 7, 14, 21 and 60 against β-actin loading control in WT and Tg21 mice. Quantification of protein expression is shown for: **b)** VDAC1, 2-way ANOVA, $F(1, 16) = 73.94$, $^{****}p < 0.0001$; **d)** mitochondrial complex I (CI), NADH dehydrogenase, subunit NDUFB8, 2-way ANOVA, $F(1,24) = 17.83$, $^{***}p = 0.0005$; **e)** mitochondrial complex II (CII), succinate dehydrogenase, 2-way ANOVA, $F(1,24) = 7.9$, $p = 0.05432$; **f)** mitochondrial complex III (CIII), 2-way ANOVA, $F(1,24) = 52.81$, $^{****}p < 0.0001$; **g)** mitochondrial complex IV (CIV), cytochrome c oxidase (COX), subunit 1, 2-way ANOVA, $F(1,24) = 94.67$, $^{****}p < 0.0001$; and **h)** mitochondrial complex V (CV), ATP synthase, alpha subunit, 2-way ANOVA, $F(1,24) = 12.15$, $^{**}p = 0.0023$. Mitochondrial protein expression is higher in Tg21 mice at P7 (CIII, CIV, and CV), P14 (VDAC1, CI and CIV), P21 (VDAC1 and CIV), and at P60 (CIV). Multiple comparisons: 2-way ANOVA: *, **, ***, ****: $p<;0.05$, $p<0.01$, $p<;0.001$, $p<0.0001$.

Figure 6. CNS EPO overexpression promotes no difference in the NADPH oxidase (NOX), superoxide dismutase 1 (SOD1) ratio. Hippocampal measures of: **a)** NOX activity, **b)** SOD activity, and **c)** the ratio of NOX/SOD1 activities in WT and Tg21 mice at postnatal ages P14 and P21 show elevated SOD activity at P14 (1-way ANOVA, $F(1,16) = 5.89$, $^{*}p = 0.02$), but no difference in the ratio of activities at either age.

Figure 7. CNS EPO overexpression enhances hippocampally dependent spatial navigation and reference memory. Outcome variables relating to the acquisition phase (left column) and reversal phase (right column) from Morris Water Maze (MWM) tests performed in WT and Tg21 mice at early adulthood (P48-60) are shown. Circular insets show the position of the hidden platform in the water maze. During acquisition **a)** escape latency (s) is quicker, 2-way ANOVA, $F(1,88) = 28.18$, ****$p < 0.0001$; **b)** swim path length (m) is equal, 2-way ANOVA, $F(1,88) = 0.85$, $p = 0.36$; and **c)** swim speed (m/s) faster, 2-way ANOVA, $F(1, 88)=624$, ****$p<0.0001$ in Tg21 mice . During reversal **d)** escape latency (s) is faster, 2-way ANOVA, $F(1,88) = 108$, ****$p < 0.0001$; **e)** swim path length (m) shorter, 2-way ANOVA, $F(1,88) = 42.1$, ****$p < 0.0001$; and **f)** Swim speed (m/s) faster, 2-way ANOVA, $F(1,88) = 185.6$, ****$p < 0.0001$). Multiple comparison: *, **, ***, ****: $p<;0.05$, $p<0.01$, $p<;0.001$, $p<0.0001$.

Figure 8. CNS EPO overexpression improves short-term memory. a) Representative diagram of the Novel Object Recognition (NOR) test, as fully explained in the methods. Object recognition relating to short-term memory function using 1h inter-trial-intervals (ITI) and long-term memory function using 24 h ITI is shown with object discrimination index. Tg21 animals demonstrated longer total exploration time and an improved discrimination index when testing short-term memory. Animals from both genotypes appeared to recognize the replaced object equally when testing long-term memory. 2-way ANOVA, $F(1,68) = 6.18$, **$p = 0.01$. **b)** T-maze working memory test shows spontaneous alternation above 75% in WT and Tg21 mice with no significant difference observed between groups. t-test, $p = 0.1329$

Figure 9. Comprehensive summer model of EPO function in the postnatal hippocampus. Panel illustration of EPO/EpoR signaling in CA1 pyramidal cells across postnatal development. EpoRs increase their expression with age and EPO activates Erk1/2 and AKT phosphorylation in these cells, leading to increased cellular respiration, mitochondrial content, and cognition.

FIGURES

Figure 1

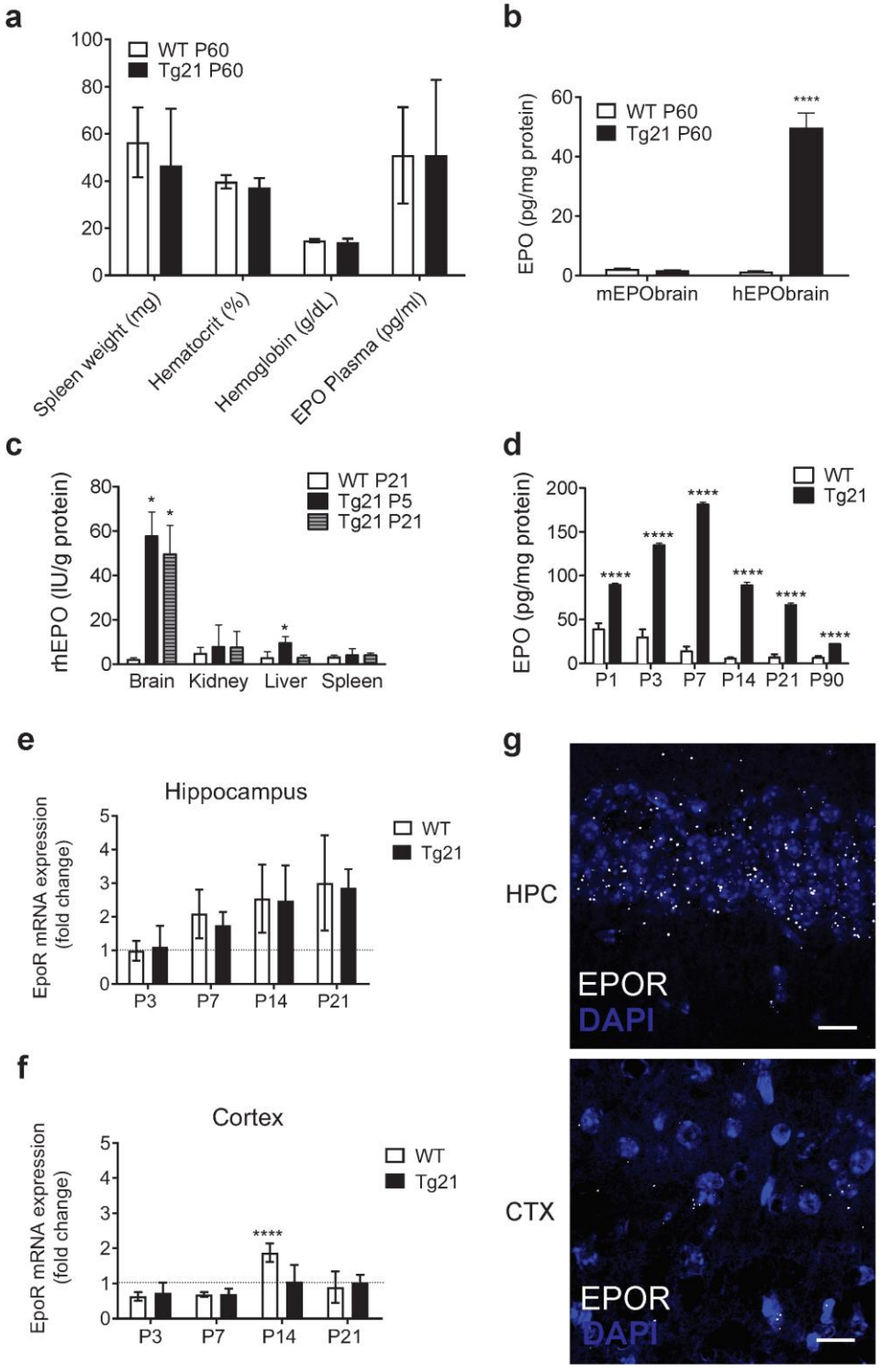

Figure 2.

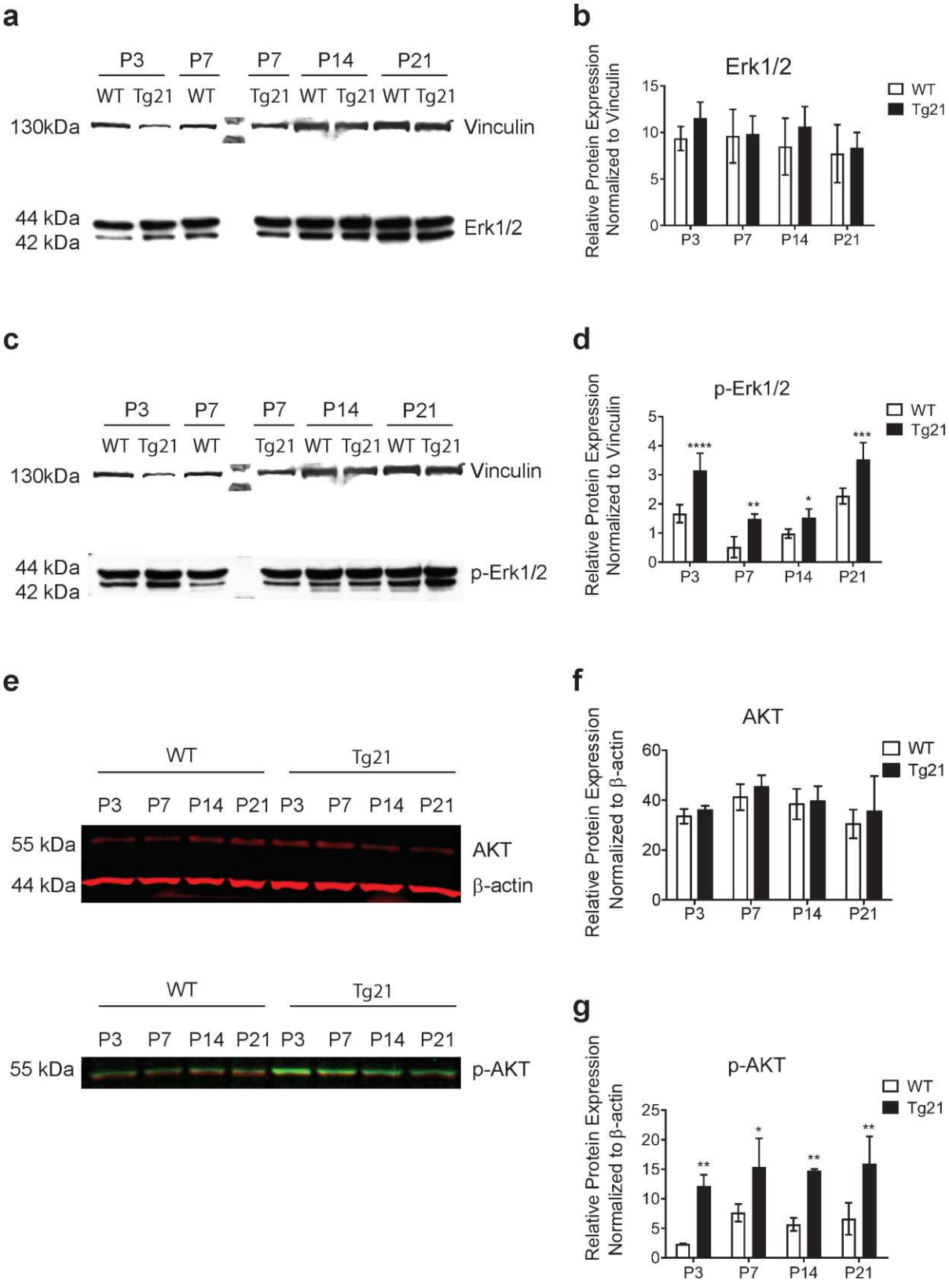
a
P3
P7
P7
P14
P21
WT Tg21 WT Tg21 WT Tg21 WT Tg21
130kDa
Vinculin
44 kDa
42 kDa
Erk1/2
b
Erk1/2
Relative Protein Expression Normalized to Vinculin
WT
Tg21
P3
P7
P14
P21
c
p-Erk1/2
d
e
WT
Tg21
55 kDa
44 kDa
AKT
β-actin
p-AKT
f
AKT
Relative Protein Expression Normalized to β-actin
g
p-AKT

Figure 3.

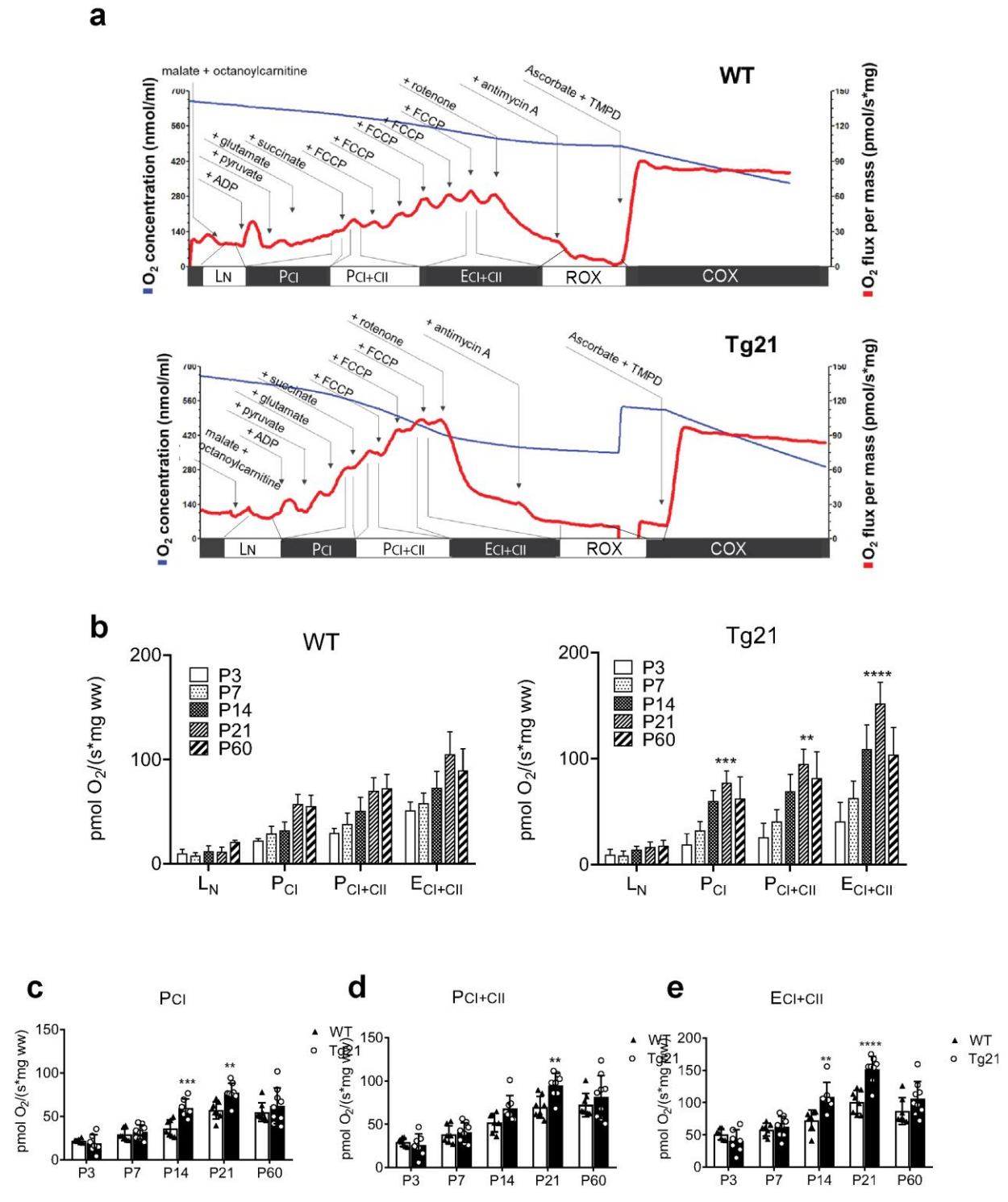
a
WT
malate + octanoylcarnitine
+ ADP
+ pyruvate
+ glutamate
+ succinate
+ FCCP
+ rotenone
+ antimycin A
Ascorbate + TMPD
O2 concentration (nmol/ml)
O2 flux per mass (pmol/s*mg)
LN
PCI
PCI+CII
ECI+CII
ROX
COX
Tg21
b
WT
Tg21
P3
P7
P14
P21
P60
pmol O2/(s*mg ww)
LN
PCI
PCI+CII
ECI+CII
c
PCI
d
PCI+CII
e
ECI+CII
WT
Tg21

Figure 4.

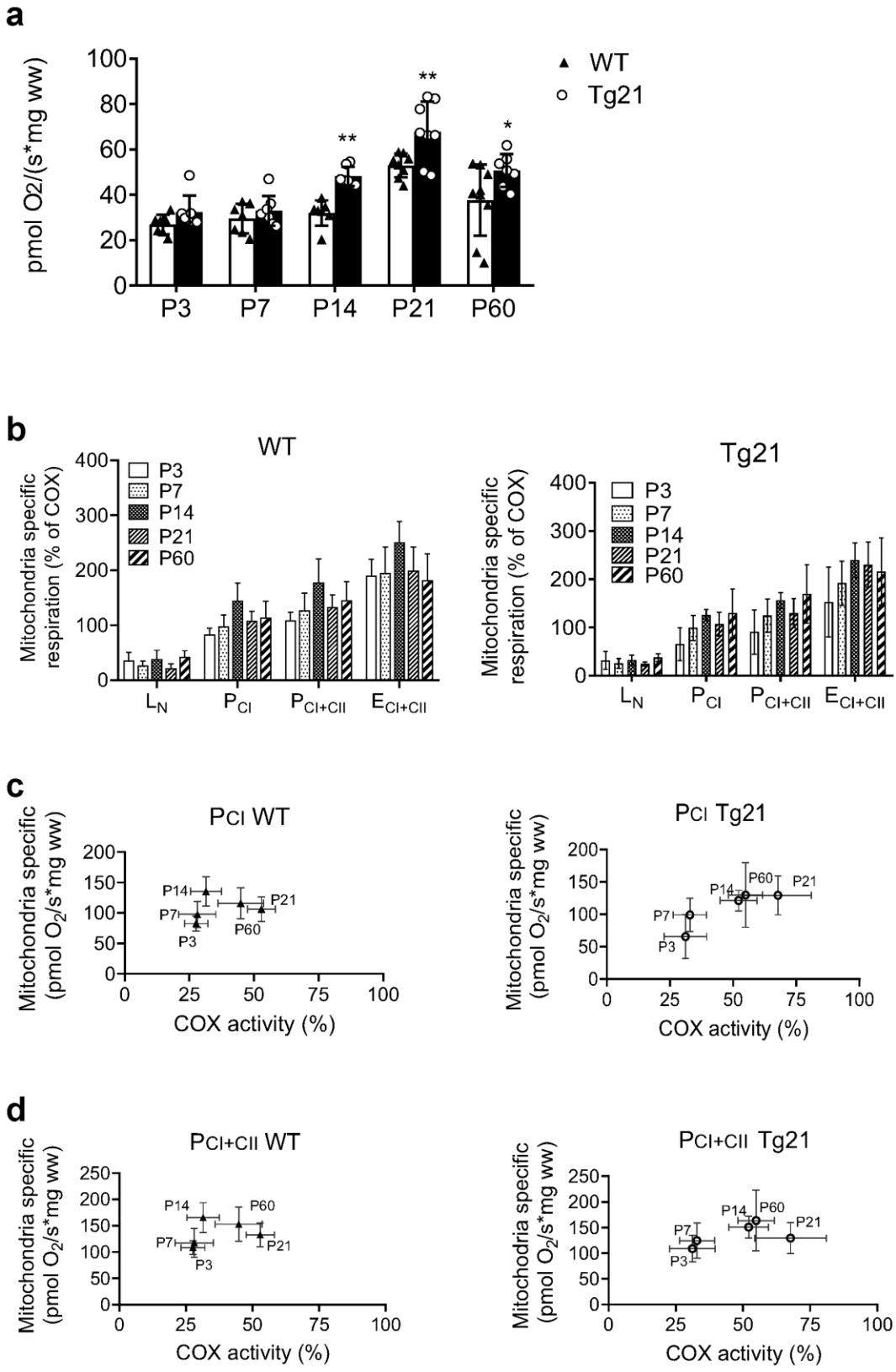
a
pmol O2/(s*mg ww)
WT
Tg21
P3
P7
P14
P21
P60
b
WT
Tg21
Mitochondria specific respiration (% of COX)
L_N
P_CI
P_CI+CII
E_CI+CII
c
PCI WT
PCI Tg21
Mitochondria specific (pmol O2/s*mg ww)
COX activity (%)
d
PCI+CII WT
PCI+CII Tg21

Figure 5.

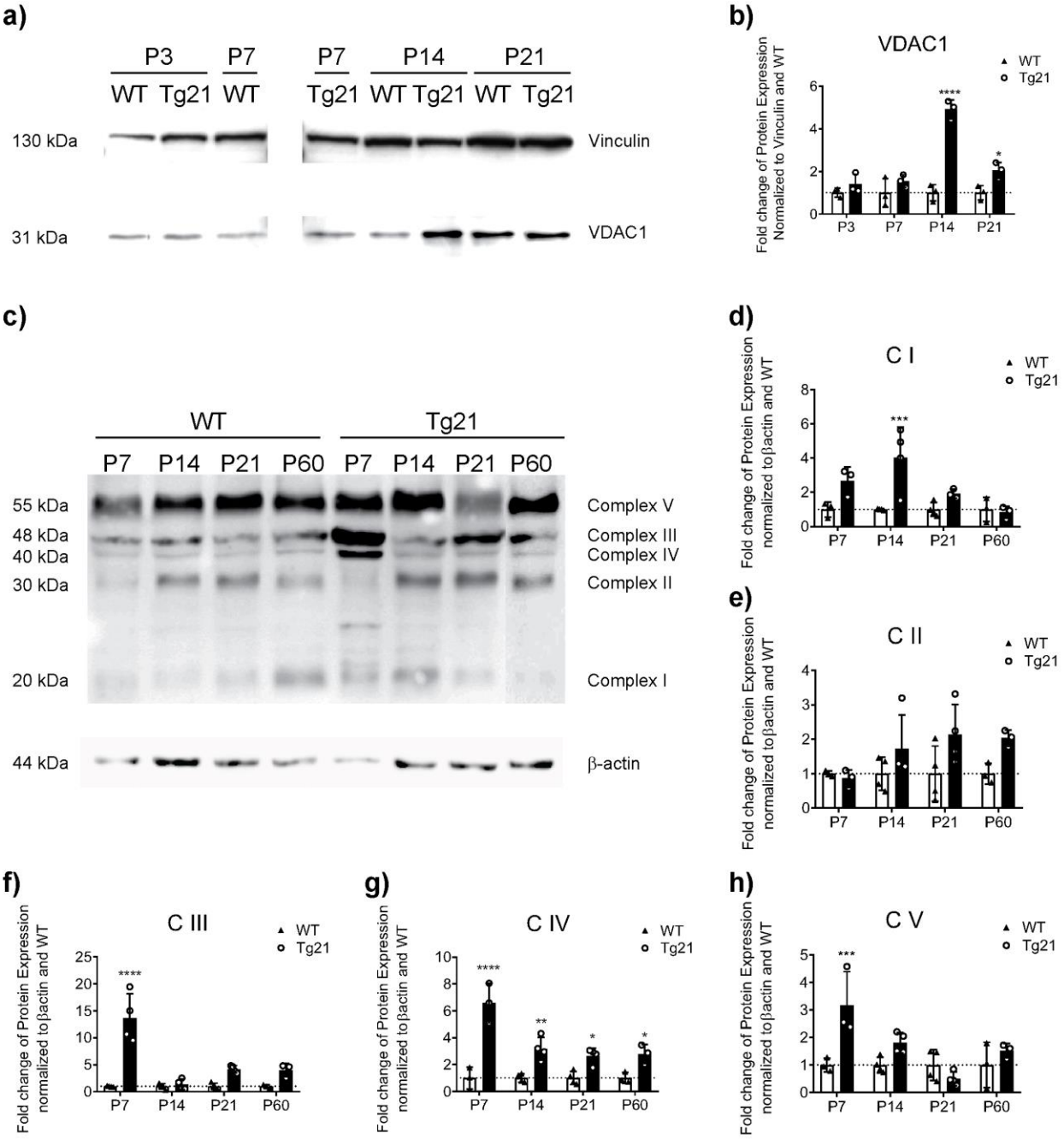
a)
P3
P7
P7
P14
P21
WT Tg21 WT Tg21 WT Tg21 WT Tg21
130 kDa
Vinculin
31 kDa
VDAC1
b)
VDAC1
WT
Tg21
Fold change of Protein Expression Normalized to Vinculin and WT
P3
P7
P14
P21
c)
WT
Tg21
P7 P14 P21 P60 P7 P14 P21 P60
55 kDa
Complex V
48 kDa
Complex III
40 kDa
Complex IV
30 kDa
Complex II
20 kDa
Complex I
44 kDa
β-actin
d)
C I
e)
C II
f)
C III
g)
C IV
h)
C V
Fold change of Protein Expression normalized to βactin and WT
P7
P14
P21
P60

Figure 6.

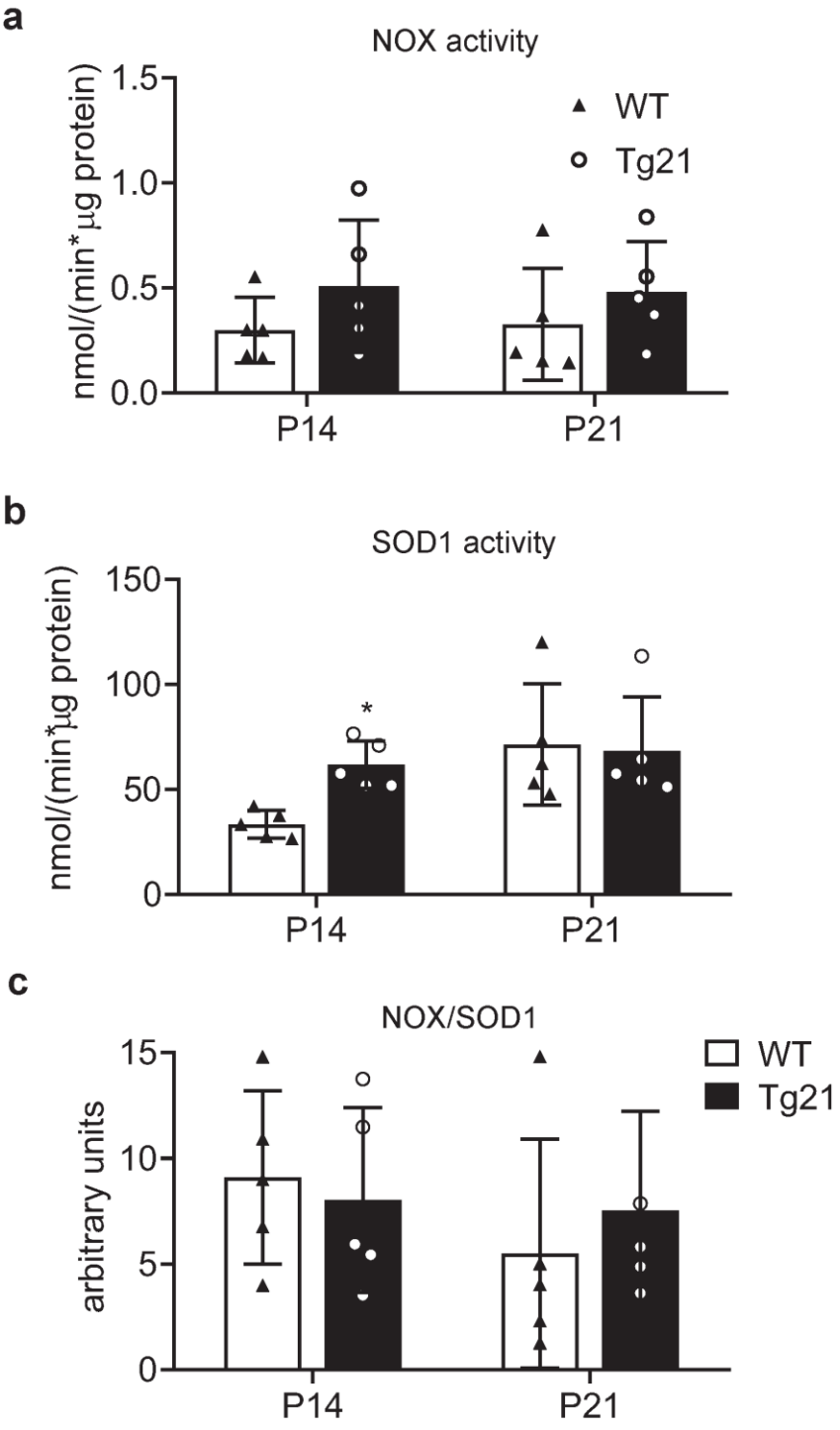
a
NOX activity
nmol/(min*µg protein)
1.5
1.0
0.5
0.0
WT
Tg21
P14
P21
b
SOD1 activity
nmol/(min*µg protein)
150
100
50
0
*
P14
P21
c
NOX/SOD1
arbitrary units
15
10
5
0
WT
Tg21
P14
P21

Figure 7.

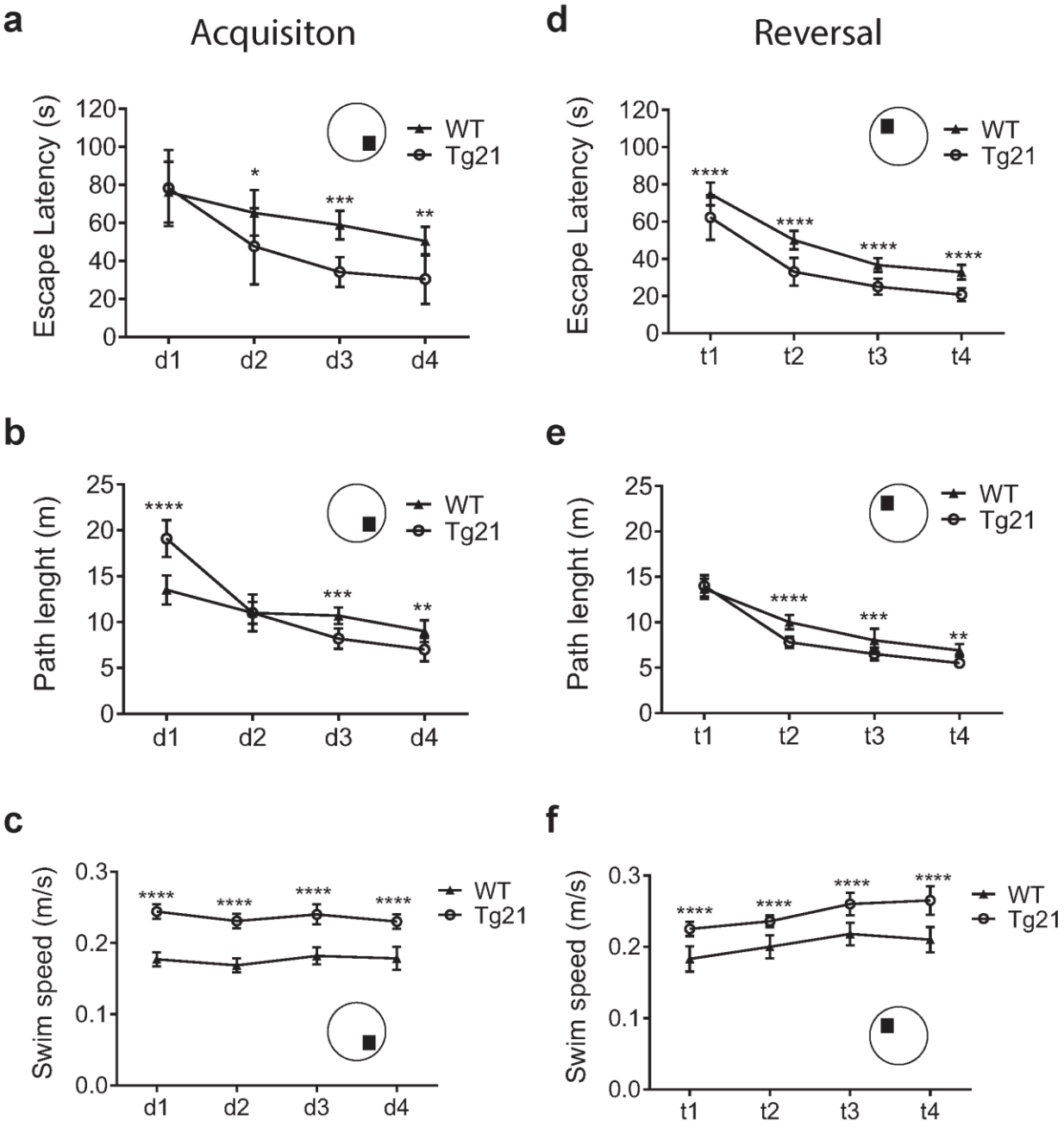
a
Acquisiton
Escape Latency (s)
120
100
80
60
40
20
0
d1
d2
d3
d4
*
***
**
WT
Tg21
d
Reversal
Escape Latency (s)
t1
t2
t3
t4
****
b
Path lenght (m)
25
20
15
10
5
e
Path lenght (m)
c
Swim speed (m/s)
0.3
0.2
0.1
0.0
f
Swim speed (m/s)

Figure 8.

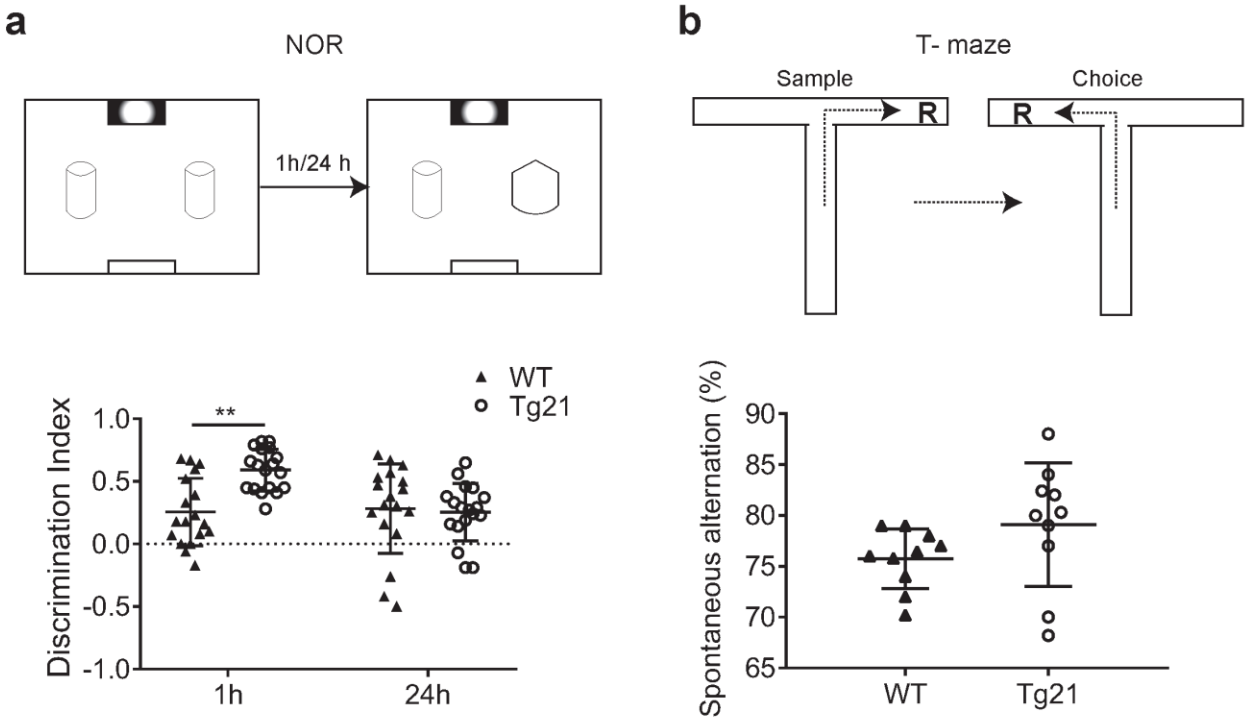
a
NOR
1h/24 h
WT
Tg21
Discrimination Index
1.0
0.5
0.0
-0.5
-1.0
**
1h
24h
b
T- maze
Sample
Choice
R
R
Spontaneous alternation (%)
90
85
80
75
70
65
WT
Tg21

Figure 9.

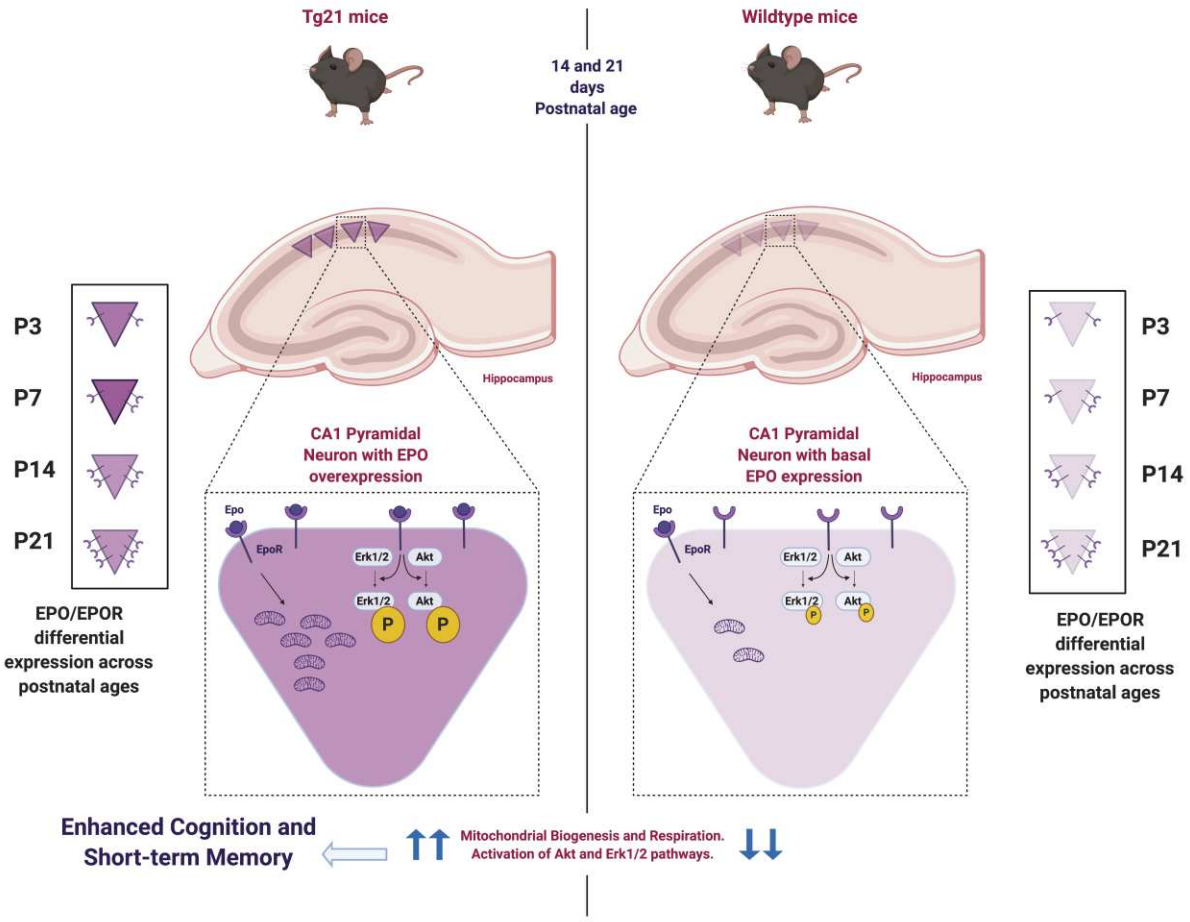
Tg21 mice
Wildtype mice
14 and 21
days
Postnatal age
P3
P7
P14
P21
EPO/EPOR
differential
expression across
postnatal ages
Hippocampus
Hippocampus
CA1 Pyramidal
Neuron with EPO
overexpression
CA1 Pyramidal
Neuron with basal
EPO expression
Epo
EpoR
Erk1/2
Akt
Erk1/2
Akt
P
P
Enhanced Cognition and
Short-term Memory
Mitochondrial Biogenesis and Respiration.
Activation of Akt and Erk1/2 pathways.

Figure S1. CNS EPO overexpression does not influence mass-specific respiratory control in cortex and brainstem. P_{CI} respiration comparisons throughout postnatal development in WT vs Tg21 mice in cortex (**a)** and brainstem (**b)**. No changes in P_{CI} were observed. Cortex: 2-way ANOVA, F(1,30) = 0.15, p = 0.699. Brainstem; 2-way ANOVA, F(1,36) = 0.0002, p = 0.99.

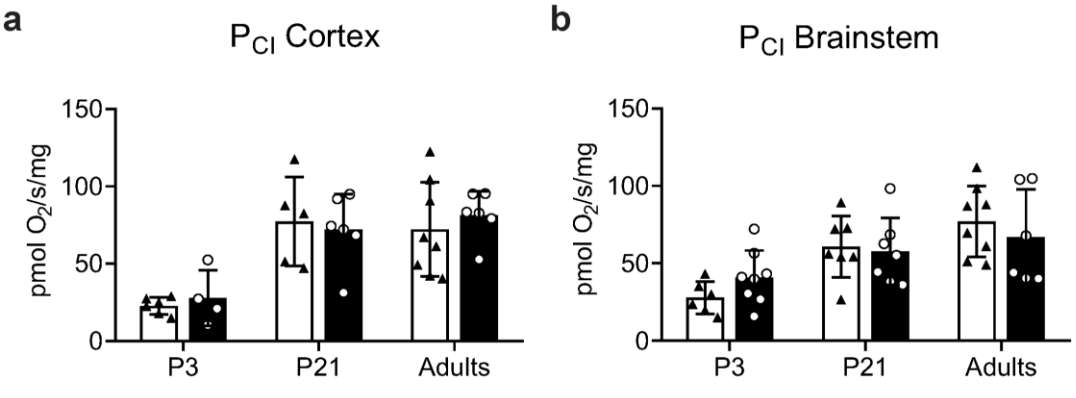

Figures

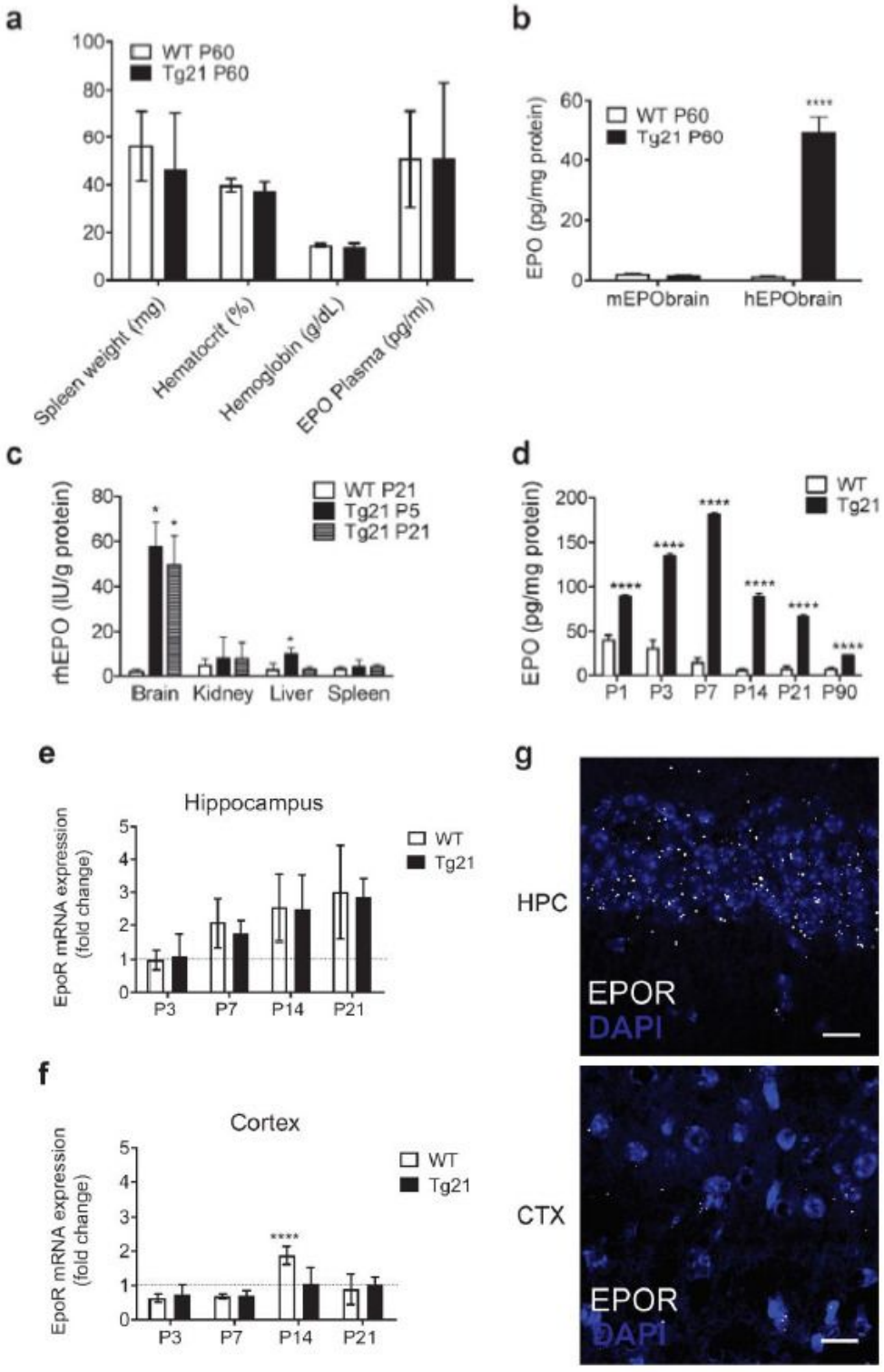

Figure 1

Overexpression of rhEPO in Tg21 mice is primarily restricted to the brain while EpoR expression in WT controls and Tg21 mice increase similarly throughout postnatal development but only in the hippocampus. a) Measures of spleen weight (mg-ww), hematocrit (%), hemoglobin (g/dL) and plasma

EPO concentration (pg/ml) at P60, showing no differences between genotypes. Student's t-test analyses; p = 0.33, spleen; p = 0.16, hematocrit; p = 0.20 hemoglobin; and p = 0.1, plasma EPO. b) Protein expression of mouse EPO (mEPO) and rhEPO in the hippocampus at P60. Negligible expression of brain mEPO is detected in either genotype whereas rhEPO expression is significantly greater in Tg21 mice. 2-way ANOVA, F(1,14) = 342, ****p < 0.0001. c) Measures of rhEPO in brain, kidney, liver, and spleen in WT and Tg21 animals at P5 and in Tg21 at P21. rhEPO overexpression is primarily isolated to the brain, with a slight (~16% of respective measure in the brain) and transient expression in the liver of Tg21 mice at P5. 1-way ANOVA, F(2,9) = 0.8, *p = 0.048. d) Total EPO protein expression (murine and recombinant human) across postnatal ages P: 1, 3, 7, 14, 21 and 90. EPO is greatly overexpressed in the hippocampus of Tg21 mice throughout postnatal development, decaying to its lowest difference (4-fold increase) respective to age-matched WT controls in adulthood (P90). 2-way ANOVA, F(1,91) = 9613, ****p < 0.0001. e) EpoR mRNA expression in the hippocampus of WT and Tg21 mice across postnatal ages P: 3, 7, 14 and 21. An age-induced increase in EpoR is shown with no difference between genotypes. 2-way ANOVA, F(3,47) = 2.767, p = 0.10. f) EpoR mRNA expression in the cortex of WT and Tg21 mice across postnatal ages P: 3, 7, 14 and 21. Primarily there is no change in EpoR expression with age or between genotypes. However, we did 49 observe a transient increase in WT mice at P14. 2-way ANOVA, F(3,47) = 18.14, ****p < 0.0001. g) Representative images of hippocampal (HPC) CA1 area and cortical L5-6 area (CTX) from young adult (P60) WT mice. EpoR mRNA expression is highly visible in HPC principal neurons whereas negligible EpoR mRNA can be seen in CTX. Scale: 20 □m.

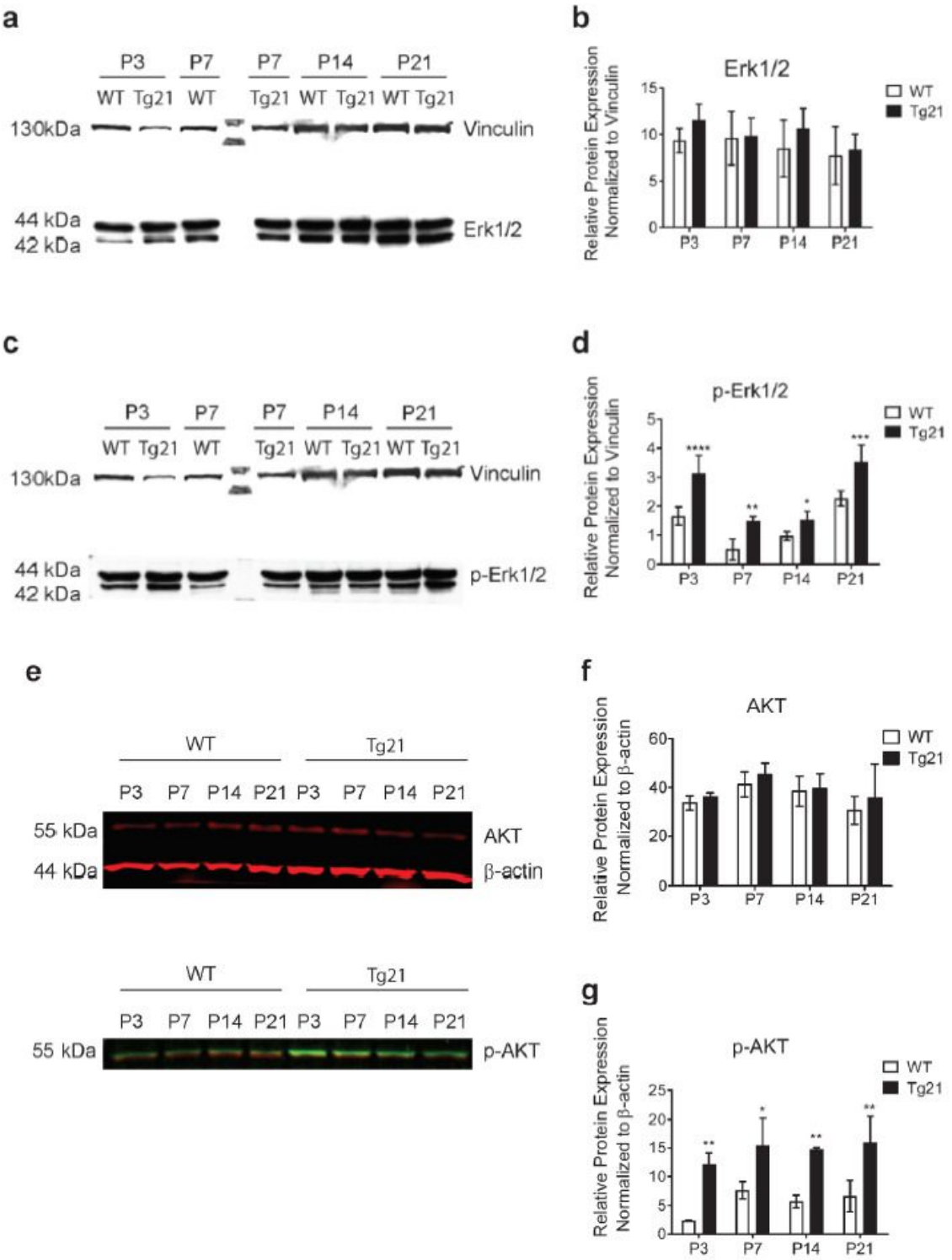

Figure 2

EPO overexpression in the central nervous system (CNS) activates Erk1/2 and AKT in the hippocampus. a) Representative images of total Erk1/2 protein expression across postnatal ages P: 3, 7, 14 and 21 in WT and Tg21 mice and vinculin loading control. b) Quantification of total Erk1/2 protein shows no change throughout development or between genotypes. 2-way ANOVA, $F(3,24) = 0.309$, $p = 0.583$. c) Phosphorylated (p-)Erk1/2 protein expression across postnatal ages P: 3, 7, 14 and 21 in WT and Tg21

mice. d) Quantification of p-Erk1/2 shows highest levels of phosphorylation at P3 and P21 in both genotypes and 2-fold higher activation in the Tg21 mice across all measured ages. 2-way ANOVA, $F(3,24) = 26.97$, ****$p < 0.0001$. Multiple comparison: *, **, ***, ****: p<;0.05, p<0.01, p<;0.001, p<0.0001. e) Representative images of total AKT protein expression with β-actin loading control (red; top) and p-AKT (green) superimposed over total AKT (bottom) in WT and Tg21 mice at postnatal ages P: 3, 7, 14, and 21. f) Quantification of total AKT shows no change throughout development or difference between genotypes. 2-way ANOVA, $F(3,24) = 1.347$, $p = 0.263$. g) Quantification of p-AKT shows the lowest levels of phosphorylation in WT mice at P3 and higher values in Tg21 mice at P3 (5-fold), P7 (3-fold), P14 (3-fold) and P21 (3-fold). 2-way ANOVA, $F(3,24) = 65.64$, ****$p < 0.0001$, multiple comparisons: *, **, p<;0.05, p<0.01.

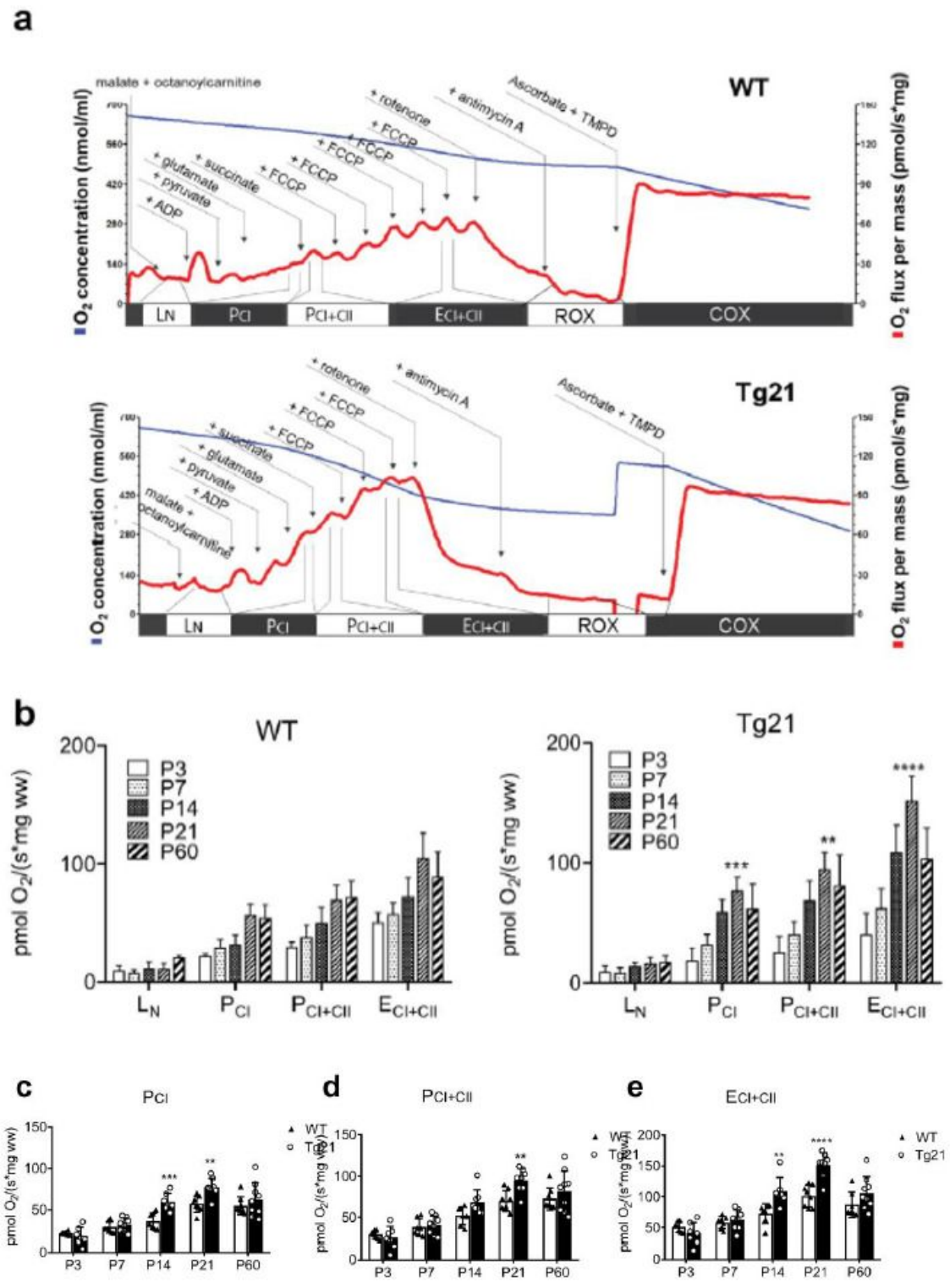

Figure 3

CNS EPO overexpression influences mass-specific respiratory control in postnatal hippocampus. a) Schematic representation of respirometric traces from a WT (top) and Tg21 (bottom) recording, which illustrate the change in oxygen concentration (nmol·ml-1, left y-axis, blue line) and oxygen flux per mass (pmol O2 / s * mg ww, right y-axis, red line) in hippocampal tissue at P21. Respiratory states were achieved through the titration of various substrates, inhibitors, as well as a protonophore. The order of

respiratory state analysis from beginning to end (left-to-right) with the respective substrates, inhibitors, or protonophores added, as fully explained in the methods, consisted of: leak without adenylates (LN, malate and octanoylcarnitine); coupled respiration with maximal electron input from mitochondrial complex I (PCI, pyruvate and glutamate); maximal rates of coupled respiration with electron input from complex I and II (PCI+CII, succinate); maximal noncoupled respiration (E) with electron input from complex I and II (ECI+CII, steps of carbonyl cyanide p-trifluoromethoxy phenylhydrazone, FCCP, addition until respiration ceases to increase); noncoupled respiration with maximal electron input from mitochondrial complex II (ECII, rotenone); and non-mitochondrial residual oxygen consumption (ROX, antimycin A). Following respiratory state analysis, ascorbate and N,N,N',N'-tetramethyl-1,4-benzenediamine, dihydrochloride (TMPD) were simultaneously added to assess cytochrome c oxidase (COX; complex IV) activity via mass-specific oxygen consumption rates (pmol O2 / s * mg ww). b) Hippocampal mass-specific oxygen consumption rates (OCR) from WT (left) and Tg21 (right) mice at postnatal ages of P: 3, 7, 14, 21, and 60. LN: 2-way ANOVA, $F(1,66) = 0.08$, $p = 0.78$; PCI: 2-way ANOVA, $F(1,66) = 15.74$, ***$p = 0.0002$; PCI+CII: 2-way ANOVA, $F(1,67) = 9.072$, **$p = 0.0037$; and ECI+CII 2-way ANOVA, $F(1,66) = 21.59$, ****$p < 0.0001$. c) PCI respiration, 51 d) PCI+CII respiration, and e) ECI+CII respiration comparisons throughout postnatal development in WT vs Tg21 mice. Tg21 mice displayed higher rates of PCI at P14 and P21, PCI+CII at P21, and ECI+CII respiration at P14 and P21. Multiple comparisons c-e: **, ***, ****: $p < 0.01$, $p < 0.001$, and $p < 0.0001$.

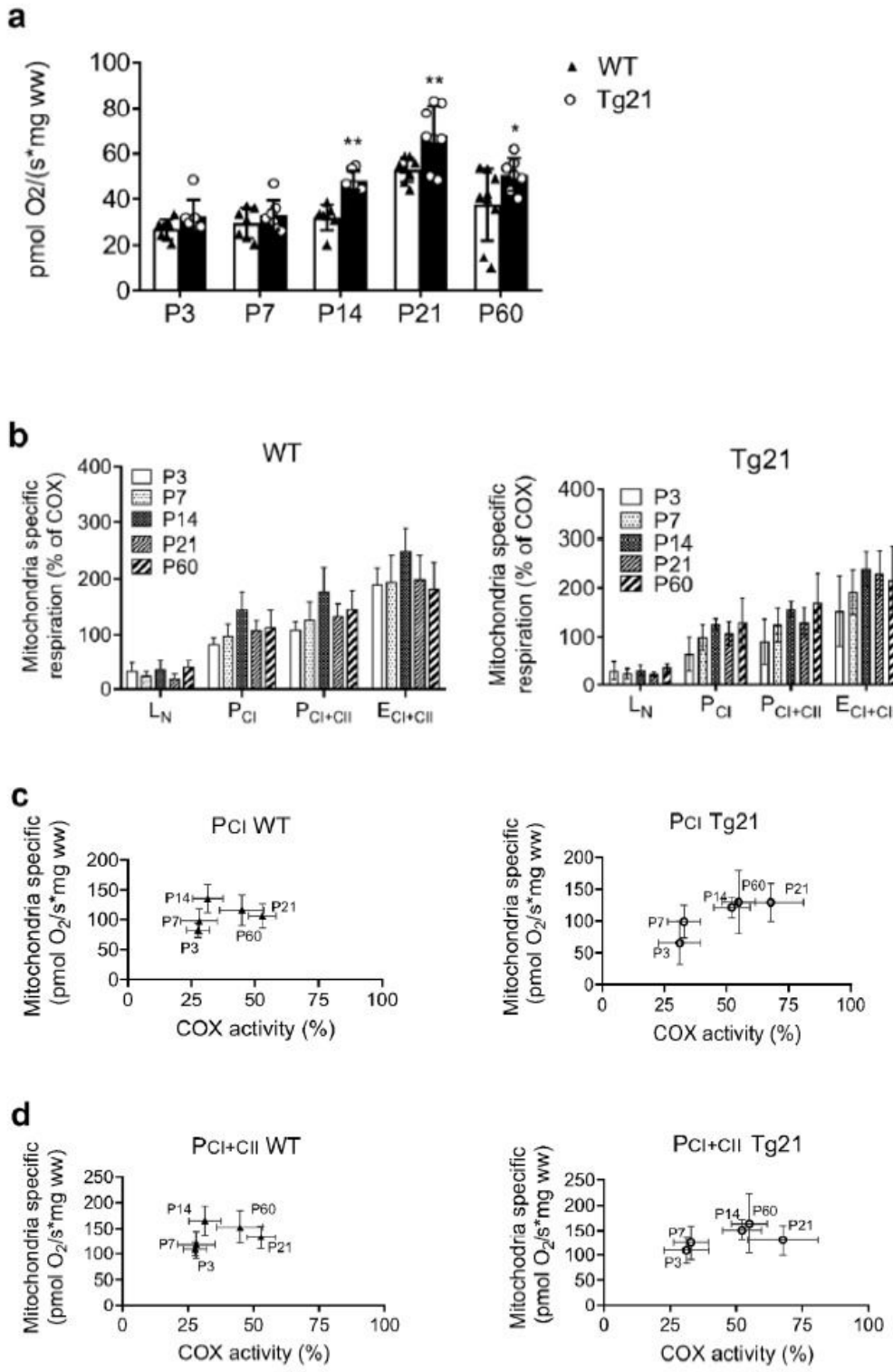

Figure 4

CNS EPO overexpression does not influence respiration when normalized to a biomarker of mitochondrial content in postnatal hippocampus. a) Cytochrome C oxidase activity (COX, pmol O2 / s * mg ww) in the hippocampus of WT and Tg21 throughout postnatal development. Tg21 mice show higher COX activity at P14, P21, and P60. 2-way ANOVA, $F(1,66) = 27.32$, ****$p < 0.0001$. Multiple comparisons: *, **: $p < 0.05$, and $p < 0.01$. b) Mass-specific oxygen consumption rates (OCR) relative to COX (%) in WT and Tg21 mice

for leak respiration without adenylates (LN); coupled respiration with maximal electron input from mitochondrial complex I (PCI); maximal rates of coupled respiration with electron input from complex I and II (PCI+CII); and maximal noncoupled respiration with electron input from complex I and II (ECI+CII). Mass-specific respiratory differences between genotypes are lost when normalizing to COX, a surrogate of mitochondrial content. c) Correlations between mitochondrial content via COX activity and mito-specific respiration for PCI and d) PCI+CII throughout postnatal development in WT (left panels) and Tg21 (right panels) mice, respectively. An increase in respiration throughout postnatal development is observed along with an increase in mitochondrial content in both genotypes for both respiratory states. Mitochondrial content is greater in at P21 and P60 in WT mice, and at P14, P21 and P60 in Tg21 mice.

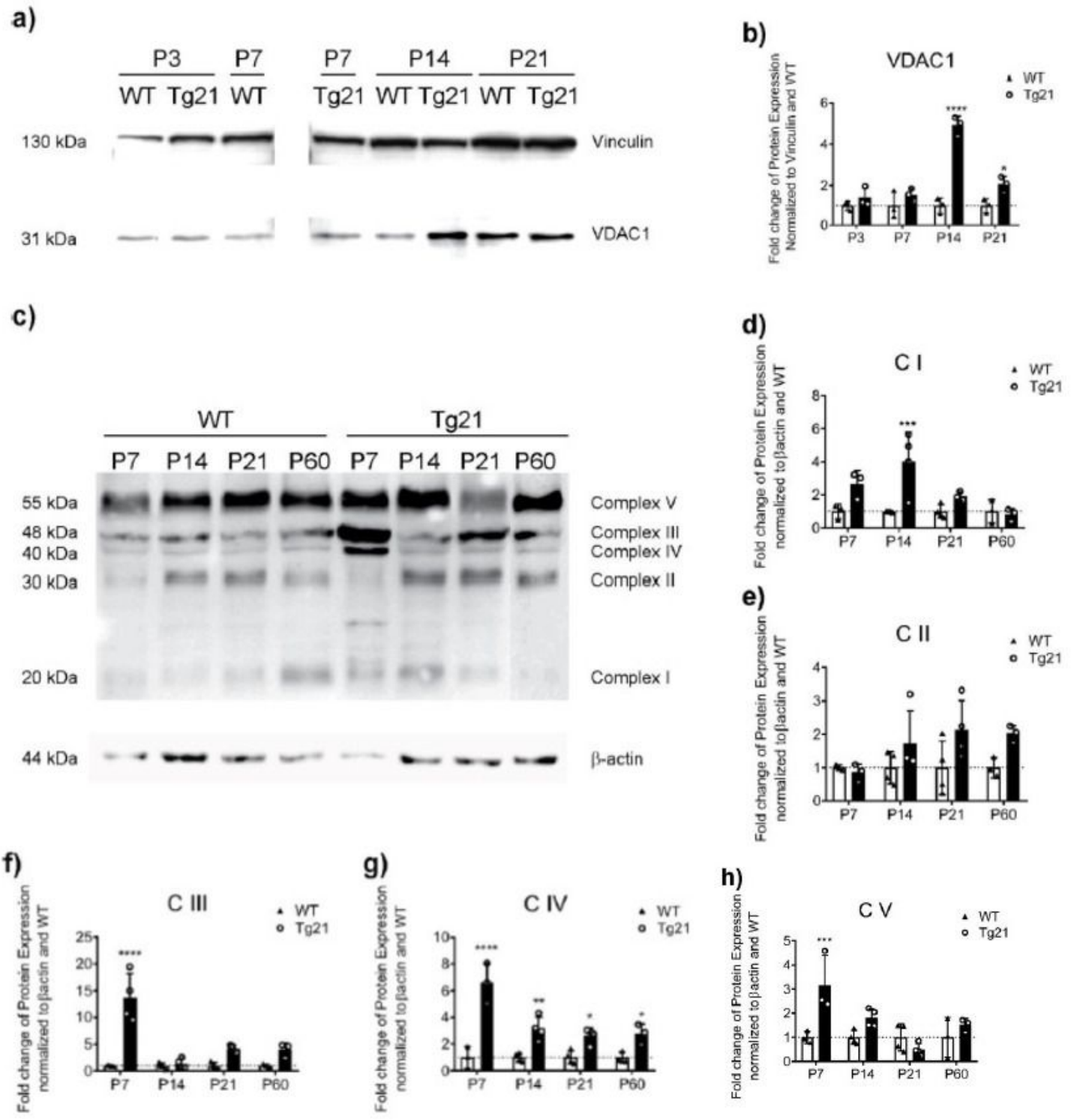

Figure 5

CNS EPO overexpression increases additional evidence of mitochondrial content in hippocampus throughout postnatal development. Representative images of: a) total voltage-dependent anion channel 1 (VDAC1) across postnatal ages P: 3, 7, 14 and 21 against vinculin loading control; and c) mitochondrial electron transport complex protein expressions across postnatal ages P: 7, 14, 21 and 60 against β-actin loading control in WT and Tg21 mice. Quantification of protein expression is shown for: b) VDAC1, 2-way ANOVA, $F(1, 16) = 73.94$, ****$p < 0.0001$; d) mitochondrial complex I (CI), NADH dehydrogenase, subunit

NDUFB8, 2-way ANOVA, F(1,24) = 17.83, ***p = 0.0005; e) mitochondrial complex II (CII), succinate dehydrogenase, 2-way ANOVA, F(1,24) = 7.9, p = 0.05432; f) mitochondrial complex III (CIII), 2-way ANOVA, F(1,24) = 52.81, ****p < 0.0001; g) mitochondrial complex IV (CIV), cytochrome c oxidase (COX), subunit 1, 2-way ANOVA, F(1,24) = 94.67, ****p < 0.0001; and h) mitochondrial complex V (CV), ATP synthase, alpha subunit, 2-way ANOVA, F(1,24) = 12.15, **p = 0.0023. Mitochondrial protein expression is higher in Tg21 mice at P7 (CIII, CIV, and CV), P14 (VDAC1, CI and CIV), P21 (VDAC1 and CIV), and at P60 (CIV). Multiple comparisons: 2-way ANOVA: *, **, ***, ****: p<;0.05, p<0.01, p<;0.001, p<0.0001.

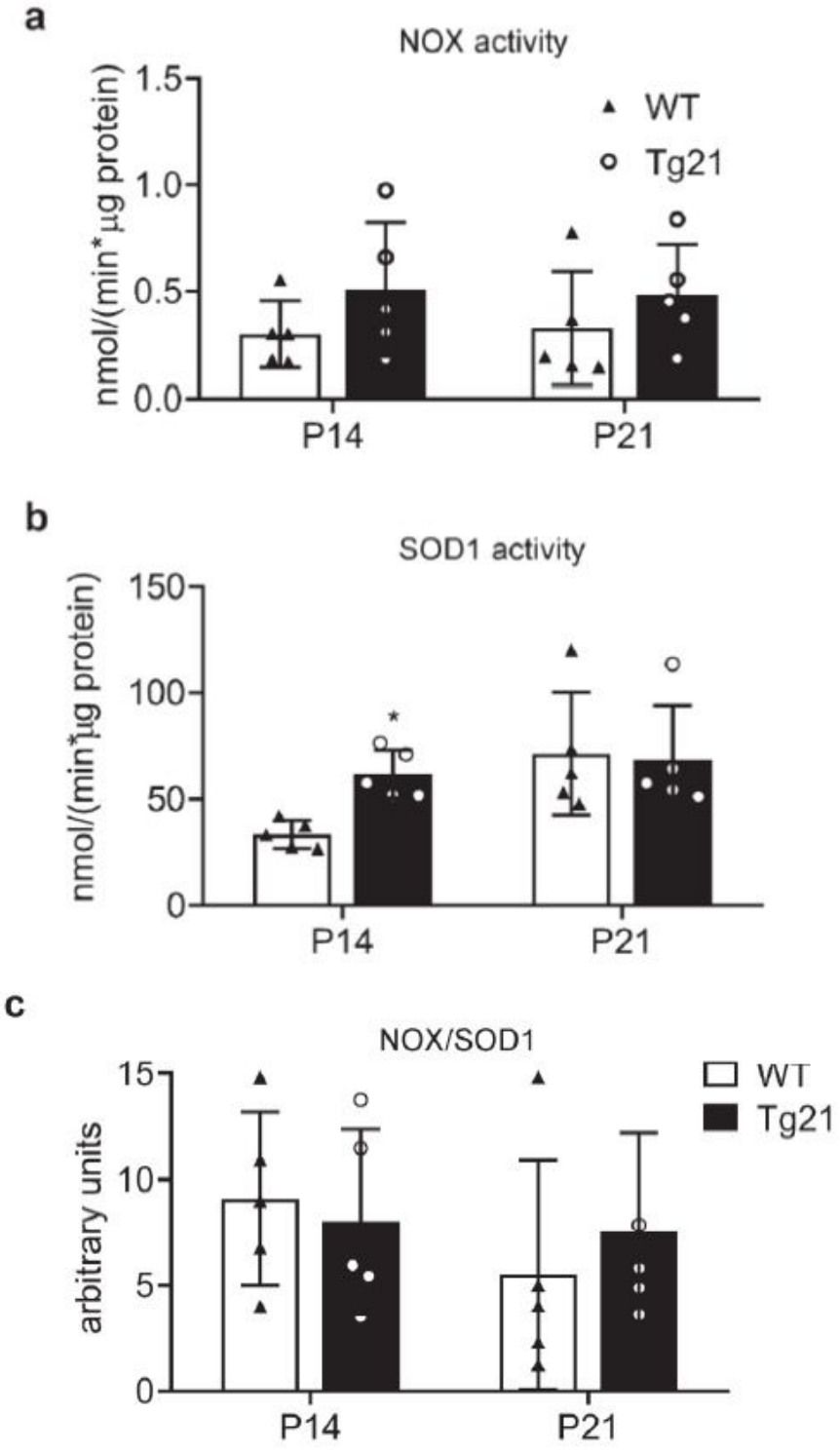

Figure 6

CNS EPO overexpression promotes no difference in the NADPH oxidase (NOX), superoxide dismutase 1 (SOD1) ratio. Hippocampal measures of: a) NOX activity, b) SOD activity, and c) the ratio of NOX/SOD1 activities in WT and Tg21 mice at postnatal ages P14 and P21 show elevated SOD activity at P14 (1-way ANOVA, $F(1,16) = 5.89$, $^*p = 0.02$), but no difference in the ratio of activities at either age.

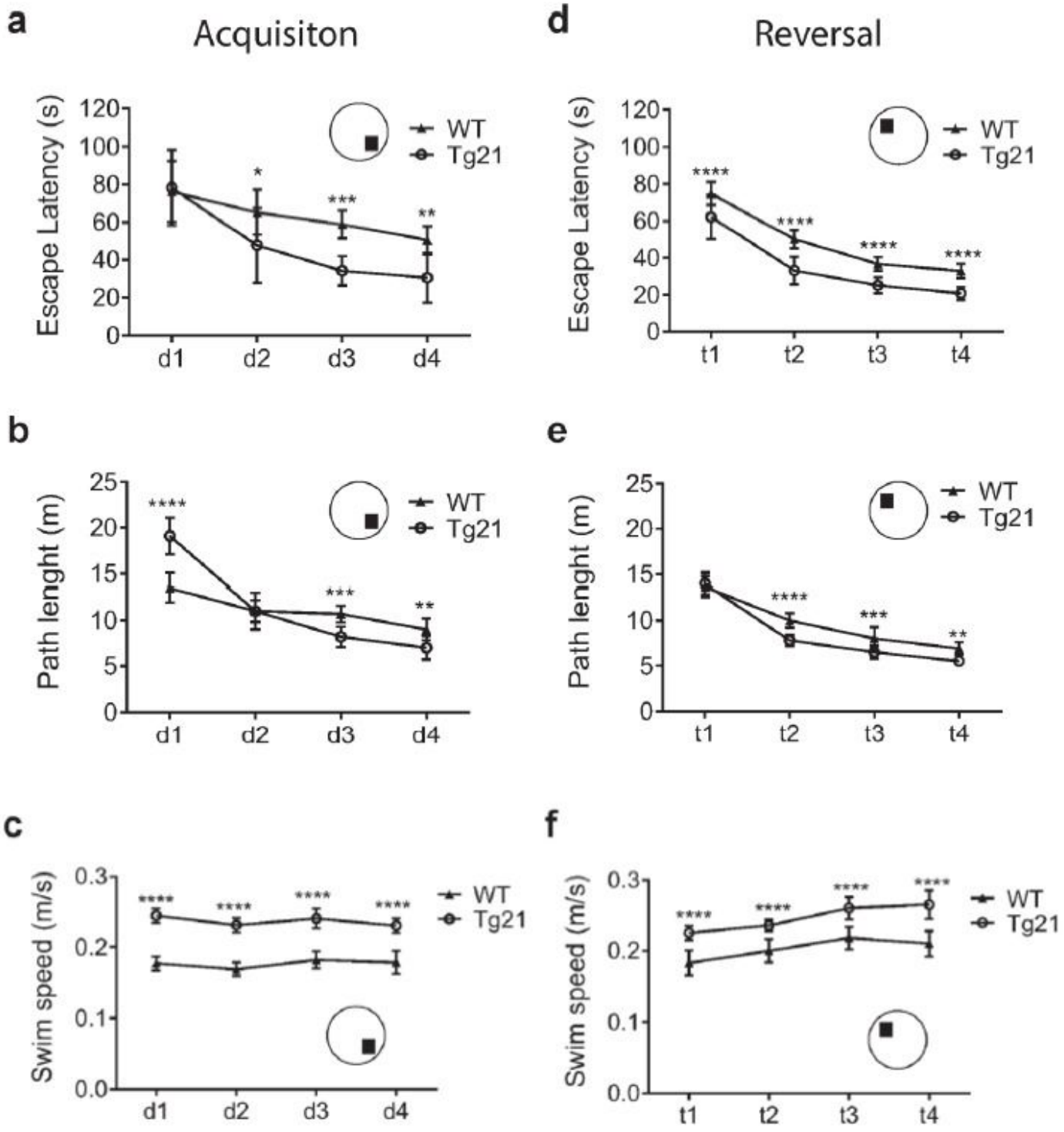

Figure 7

CNS EPO overexpression enhances hippocampally dependent spatial navigation and reference memory. Outcome variables relating to the acquisition phase (left column) and reversal phase (right column) from Morris Water Maze (MWM) tests performed in WT and Tg21 mice at early adulthood (P48-60) are shown. Circular insets show the position of the hidden platform in the water maze. During acquisition a) escape latency (s) is quicker, 2-way ANOVA, F(1,88) = 28.18, ****p < 0.0001; b) swim path length (m) is equal, 2-way ANOVA, F(1,88)= 0.85, p = 0.36; and c) swim speed (m/s) faster, 2-way ANOVA, F(1, 88)=624, ****p<0.0001 in Tg21 mice . During reversal d) escape latency (s) is faster, 2-way ANOVA, F(1,88) = 108, ****p < 0.0001; e) swim path length (m) shorter, 2-way ANOVA, F(1,88) = 42.1, ****p < 0.0001; and f) Swim speed (m/s) faster, 2-way ANOVA, F(1,88) = 185.6, ****p < 0.0001). Multiple comparison: *, **, ***, ****: p<;0.05, p<0.01, p<;0.001, p<0.0001.

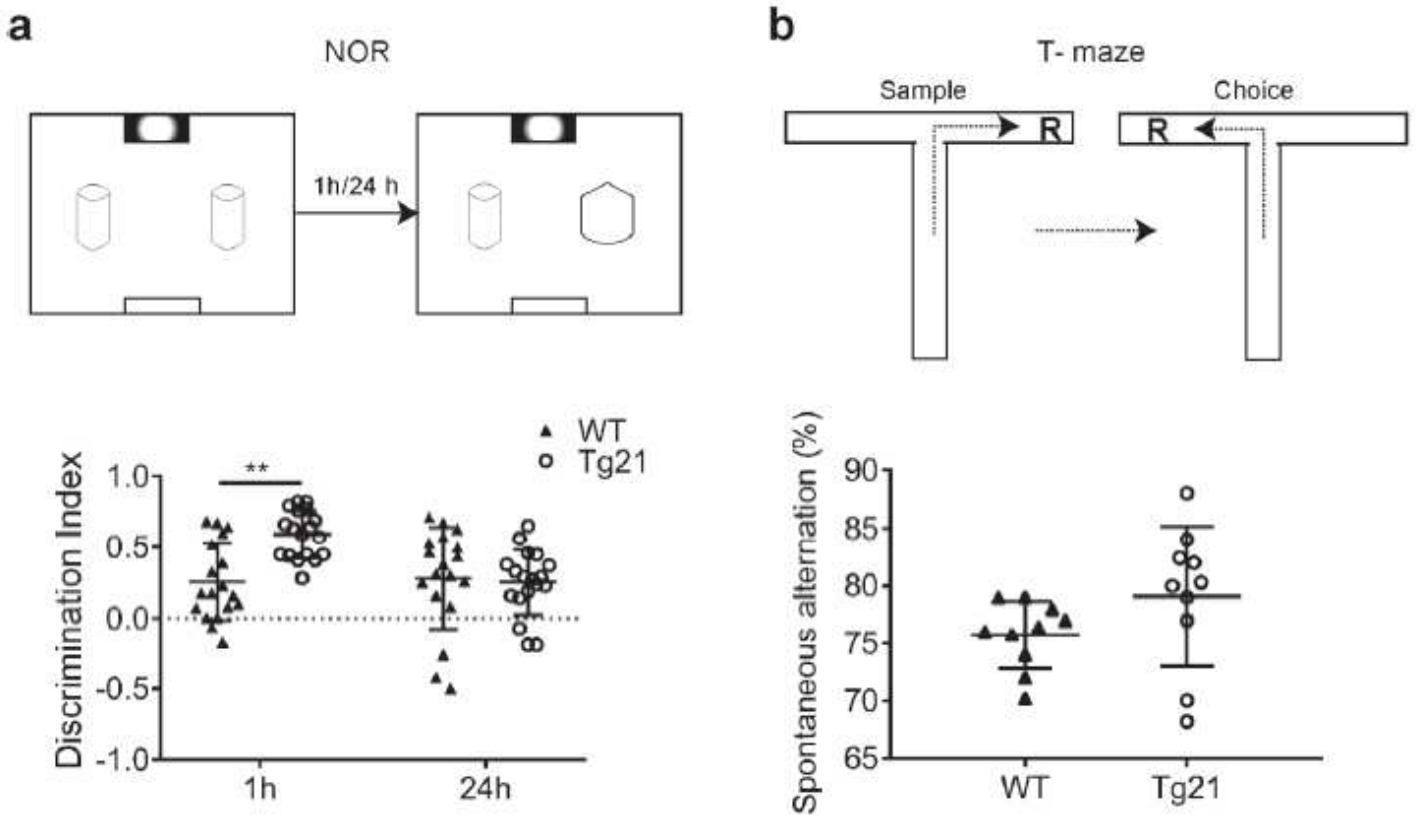

Figure 8

CNS EPO overexpression improves short-term memory. a) Representative diagram of the Novel Object Recognition (NOR) test, as fully explained in the methods. Object recognition relating to short-term memory function using 1h inter-trial-intervals (ITI) and long-term memory function using 24 h ITI is shown with object discrimination index. Tg21 animals demonstrated longer total exploration time and an improved discrimination index when testing short-term memory. Animals from both genotypes appeared to recognize the replaced object equally when testing long-term memory. 2-way ANOVA, F(1,68) = 6.18, **p = 0.01. b) T-maze working memory test shows spontaneous alternation above 75% in WT and Tg21 mice with no significant difference observed between groups. t-test, p = 0.1329

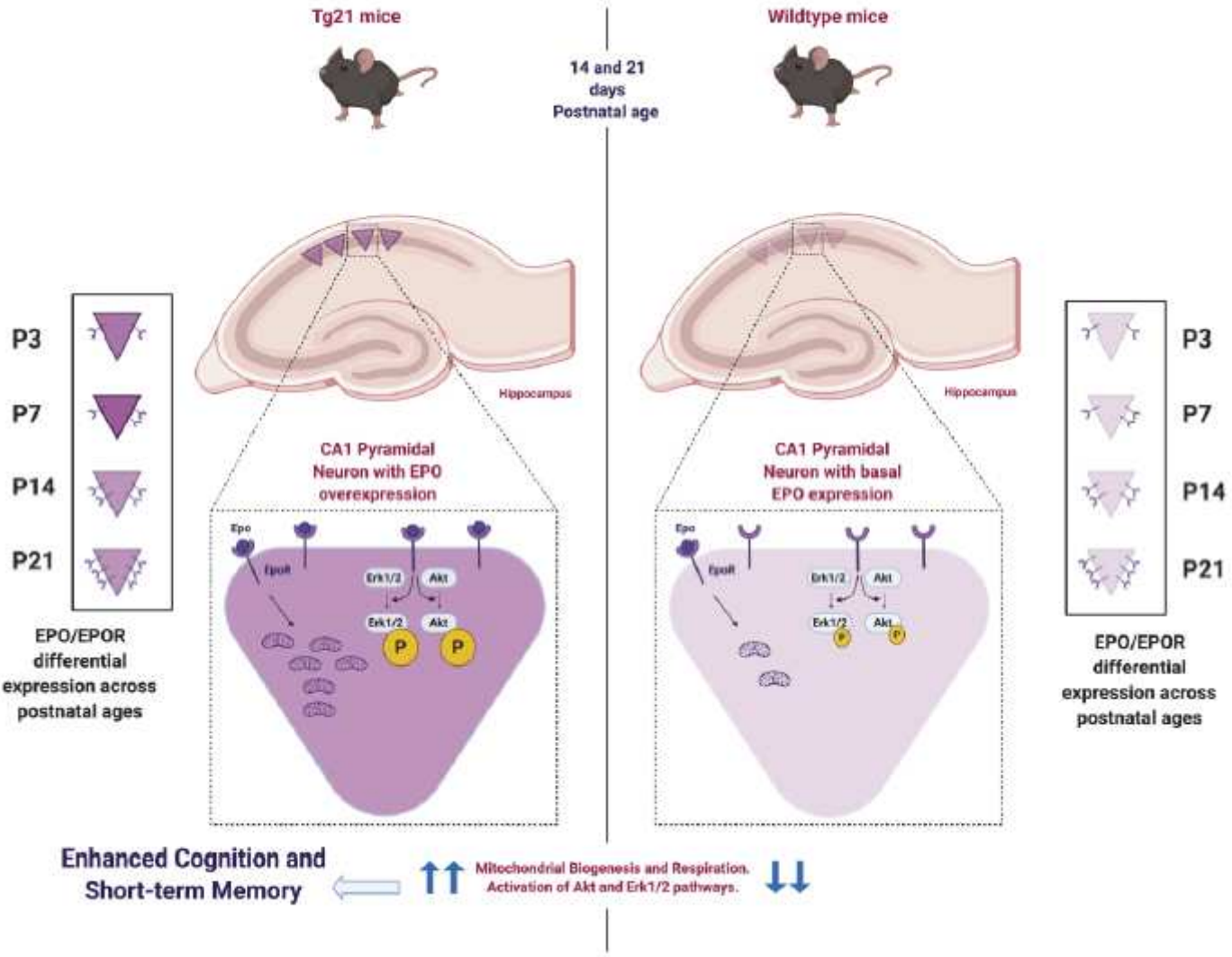

Figure 9

Comprehensive summer model of EPO function in the postnatal hippocampus. Panel illustration of EPO/EpoR signaling in CA1 pyramidal cells across postnatal development. EpoRs increase their expression with age and EPO activates Erk1/2 and AKT phosphorylation in these cells, leading to increased cellular respiration, mitochondrial content, and cognition.

Supplementary Files

This is a list of supplementary files associated with this preprint. Click to download.

- FigS1.png